NAVAL POSTGRADUATE SCHOOL
Monterey, California

DISSERTATION

ANALYTIC EXPRESSION OF THE BUCKLING LOADS FOR STIFFENED PLATES WITH BULB-FLAT FLANGES

by

Archie Wilmer III

June 2003

Dissertation Supervisor: Don Danielson

THIS PAGE INTENTIONALLY LEFT BLANK

REPORT DOCUMENTATION PAGE			Form Approved OMB No. 0704-0188
Public reporting burden for this collection of information is estimated to average 1 hour per response, including the time for reviewing instruction, searching existing data sources, gathering and maintaining the data needed, and completing and reviewing the collection of information. Send comments regarding this burden estimate or any other aspect of this collection of information, including suggestions for reducing this burden, to Washington headquarters Services, Directorate for Information Operations and Reports, 1215 Jefferson Davis Highway, Suite 1204, Arlington, VA 22202-4302, and to the Office of Management and Budget, Paperwork Reduction Project (0704-0188) Washington DC 20503.			
1. AGENCY USE ONLY *(Leave blank)*	**2. REPORT DATE** June 2003	**3. REPORT TYPE AND DATES COVERED** Dissertation	
4. TITLE AND SUBTITLE: Title (Mix case letters) Analytic Expression of the Buckling Loads for Stiffened Plates with Bulb-Flat Flanges			**5. FUNDING NUMBERS**
6. AUTHOR(S) Archie Wilmer III			
7. PERFORMING ORGANIZATION NAME(S) AND ADDRESS(ES) Naval Postgraduate School Monterey, CA 93943-5000			**8. PERFORMING ORGANIZATION REPORT NUMBER**
9. SPONSORING / MONITORING AGENCY NAME(S) AND ADDRESS(ES) N/A			**10. SPONSORING / MONITORING AGENCY REPORT NUMBER**
11. SUPPLEMENTARY NOTES The views expressed in this thesis are those of the author and do not reflect the official policy or position of the Department of Defense or the U.S. Government.			
12a. DISTRIBUTION / AVAILABILITY STATEMENT Approved for public release; distribution is unlimited			**12b. DISTRIBUTION CODE** A

13. ABSTRACT ***(maximum 200 words)***

The subject of this research is the buckling behavior of a simply supported rectangular plate, with a bulb-flat stiffener attached to one side of the plate. The plate structure is subjected to axial compression that increases to the buckling load. The stiffener cross-section has a thin web and a bulb-flat flange that extends to one side of the web. Results of the investigation include planar property formulas for the asymmetric flange geometry, an analytic expression for the Saint Venant torsional constant of the flange cross-section, and an analytic expression for the buckling load corresponding to a tripping mode of the structure. The torsional constant for the bulb-flat stiffener is 15% - 23% higher than understood previously. The analytic expression for the buckling load of the bulb-flat stiffened plates considered in this investigation yields values that are 2% - 6% higher than finite element results. It is also shown that the buckling load of a plate with a bulb-flat stiffener is 3% - 4% less than that of a plate with a T-flange stiffener with the same cross-sectional area. At the onset of stiffener tripping, the torsionally superior bulb-flat tends to bend laterally, while the flexurally superior T-flange tends to twist.

14. SUBJECT TERMS Stiffened Plates, Bulb-Flat, Torsion, Saint Venant, Buckling Load			**15. NUMBER OF PAGES** 121
			16. PRICE CODE
17. SECURITY CLASSIFICATION OF REPORT Unclassified	**18. SECURITY CLASSIFICATION OF THIS PAGE** Unclassified	**19. SECURITY CLASSIFICATION OF ABSTRACT** Unclassified	**20. LIMITATION OF ABSTRACT** UL

NSN 7540-01-280-5500 Standard Form 298 (Rev. 2-89)
Prescribed by ANSI Std. 239-18

THIS PAGE INTENTIONALLY LEFT BLANK

Approved for public release; distribution is unlimited

ANALYTIC EXPRESSION OF THE BUCKLING LOADS FOR STIFFENED PLATES WITH BULB-FLAT FLANGES

Archie Wilmer III
Lieutenant Colonel, United States Army
B.S., United States Military Academy, 1982
M.S., Naval Postgraduate School, 1994

Submitted in partial fulfillment of the
requirements for the degree of

DOCTOR OF PHILOSOPHY IN APPLIED MATHEMATICS

from the

NAVAL POSTGRADUATE SCHOOL
June 2003

Author: Archie Wilmer III

Approved by:

Don Danielson
Professor of Mathematics
Dissertation Supervisor/Committee Chair

David Canright
Professor of Mathematics

Young Kwon
Professor of Mech. Eng.

Fariba Fahroo
Professor of Mathematics

Wei Kang
Professor of Mathematics

Approved by: Clyde Scandrett, Chair, Department of Mathematics

Approved by: Carson K. Eoyang, Associate Provost for Academic Affairs

THIS PAGE INTENTIONALLY LEFT BLANK

ABSTRACT

The subject of this research is the buckling behavior of a simply supported rectangular plate, with a bulb-flat stiffener attached to one side of the plate. The plate structure is subjected to axial compression that increases to the buckling load. The stiffener cross-section has a thin web and a bulb-flat flange that extends to one side of the web. Results of the investigation include planar property formulas for the asymmetric flange geometry, an analytic expression for the Saint Venant torsional constant of the flange cross-section, and an analytic expression for the buckling load corresponding to a tripping mode of the structure. The torsional constant for the bulb-flat stiffener is 15% - 23% higher than understood previously. The analytic expression for the buckling load of the bulb-flat stiffened plates considered in this investigation yields values that are 2% - 6% higher than finite element results. It is also shown that the buckling load of a plate with a bulb-flat stiffener is 3% - 4% less than that of a plate with a T-flange stiffener with the same cross-sectional area. At the onset of stiffener tripping, the torsionally superior bulb-flat tends to bend laterally, while the flexurally superior T-flange tends to twist.

THIS PAGE INTENTIONALLY LEFT BLANK

TABLE OF CONTENTS

THIS PAGE INTENTIONALLY LEFT BLANK

LIST OF FIGURES

THIS PAGE INTENTIONALLY LEFT BLANK

LIST OF TABLES

ACKNOWLEDGMENTS

I praise God, Christ Jesus, from whom all blessings flow.

I acknowledge the assistance of Professor Don Danielson who supervised this work and to whom I am deeply grateful. His expert advice and mentoring support are sincerely appreciated. I acknowledge and am truly appreciative for the intellectual support and camaraderie of Commander Vince VanJoolen and Professor Bard Mansager. Their fellowship during the pursuit of this degree was priceless. I acknowledge the support of Dr. David Kihl of the Naval Surface Warfare Center, Carderock Division, for his interest and suggestions. I thank Geoff Lofthouse and Barb Johnson, Corus Group, for their interest and support. I thank Cassandra Radigan, Patran/Nastran university coordinator, Joe Satkunknanthan, Patran/Nastran technician, Debbi Kreider, and Ron Del Presto, computer specialists, for their helpful assistance.

I am also grateful to Greater Victory Temple, COGIC of Seaside, pastor Bishop W.W. Hamilton, and First Baptist Church of Pacific Grove, pastor Reverend James Calloway for their spiritual support. I acknowledge the many family, friends, and others who have prayed and encouraged me in this undertaking.

Dedicated to my loving wife LaTressia and my darling daughter Sterling, thank you for your love, prayers, and sacrifices.

THIS PAGE INTENTIONALLY LEFT BLANK

EXECUTIVE SUMMARY

Understanding the elastic stability of stiffened plate structures is of great interest in the design of bridges, buildings, automobiles, aircraft, naval vessels, and offshore platforms. This work contributes formulas intended for the mechanical engineer, analyst, and educator involved in the analysis or design of the bulb-flat cross-section and simply supported stiffened rectangular plate.

Chapter I comments on the intent and synopsis of this investigation. Brief comments address the background for the study and literature search for published material related to the investigation. A list of notation and conventions is included.

Chapter II presents the application of multivariable calculus to derive planar property formulas for the bulb-flat cross-section. Appendices A and B contain additional derivations and expressions related to the formulas. The torsional constant is one of the key property values involved in the analysis of stiffened plate structures. No exact expression exists in published literature for the torsional constant of the bulb-flat cross-section. Saint Venant's work on an approximate expression for the torsional constant of a solid cross-section provides a method to develop an accurate one-term approximate formula applicable to bulb-flat cross-sections produced by Corus Group, one of the world's leading producers of bulb-flat profiled metals. Presented is a discussion on the idealization method to approximate the torsional constant.

Chapter III presents the application of elasticity theory and energy methods to derive a general expression for the buckling load due to the stiffener tripping of a simply supported rectangular stiffened plate subjected to axial compression. The general expression for the buckling load involves a constant called μ. The buckling load and μ values are determined graphically. The value of μ indicates the stiffener deflection behavior at the onset of stiffener tripping. Three special expressions provide initial approximations for the upper bound of the critical buckling load value. Concepts applied in the derivation include extremum principles in mechanics, the energy criterion, calculus

of variations, the Rayleigh-Ritz method, and other topics in applied mathematics and physics. The chapter also presents finite element analyses of several stiffened plate models. The results are compared to predictions made using derived formulas. MSC Nastran 2001/Patran 2001 r3 finite element software and the Maple 8 computer environment are the primary analysis and computational tools used in this investigation. Appendix C contains data tables used to represent the finite element models.

Chapter IV summarizes the major findings and conclusions of this work. This investigation:

- Determines boundary equations for the bulb-flat flange cross-section.
- Derives planar property value expressions.
- Determines an approximate torsional constant expression that is more accurate than idealizing.
- Demonstrates that the torsional property of the bulb-flat stiffener is better than previously understood. The torque-carrying capacity of a bulb-flat stiffener (possessing no structural flaws) is greater than that of an area-equivalent angle stiffener.
- Derives a general expression to predict the buckling load due to stiffener tripping of a simply supported rectangular stiffened plate subjected to axial compression. The predicted value is less than 6% higher than the finite element result.
- Demonstrates that the buckling behavior of the bulb-flat stiffened plate is unlike that of the T-flange configuration. The bulb-flat tends to buckle laterally and have a lower buckling load value than an area-equivalent T-flange stiffened plate.

Chapter IV lists future research directions that include:

- Investigating methods to determine the μ value by other than graphical means.
- Investigating the use of conformal mapping to determine the exact expression for the bulb-flat torsional constant.
- Investigating solutions to the torsion problem for asymmetric cross-sections.

- Conducting investigations of other flange cross-sections, multiple stiffener configurations, and grillages.
- Conducting further investigations of the T flange by treating the flange as a thin web plate strip instead of a beam. This treatment may achieve more accurate predictions for the T-flange buckling loads.
- Developing algorithms that increase efficiency in stiffened plate analysis and design.

THIS PAGE INTENTIONALLY LEFT BLANK

I. INTRODUCTION

A. INTENT AND SYNOPSIS

This work presents an investigation into the structural behavior and collapse of a stiffened plate panel where the stiffener is thin-webbed and the flange of the stiffener has a bulb-flat cross-section. Chapter I includes brief comments on the background and motivation for the study. Chapter II presents analytic expressions for the cross-sectional properties of the bulb-flat flange. For brevity, Appendices A and B contain key derivations related to the property expressions. Cross-sectional properties include area, centroid, moments of inertia, and torsional constant. The property values for the flange cross-section are needed in the analytic formulas to determine the buckling load of the stiffened plate. Chapter II presents a comparison of the bulb-flat stiffener configuration to the angle flange configuration to show that the torsional property of the bulb-flat stiffener is better than previously understood. Chapter III presents a comparison of the bulb-flat stiffened plate configuration to the T-flange configuration to show that their buckling behaviors are different given the same cross-sectional area. These comparisons provide better discernment of the buckling characteristics of stiffened plates. Chapter III contains the development of a buckling load formula for a stiffened plate resulting from stiffener tripping. The onset of stiffener tripping negates the stiffener's support to the plate panel and leads to eventual collapse of the structure. The aim is to develop an analytic expression for the buckling load of a rectangular stiffened plate, with one or more parallel bulb-flat stiffeners attached to one side, where the plate structure is subjected to axial compression. The focus of the analysis is on a rectangular plate stiffened with one bulb-flat stiffener. The results can be extended and applied to plate structures with more than one stiffener. Energy methods are used, as an alternative to vector methods, to analyze the displacement and deflection behavior of the stiffened plate model. The chapter contains finite element analyses of several stiffened plate models using MSC Nastran 2001/Patran 2001-r3 software. Finite element analysis results are compared to formula results to assess formula accuracy and the validation of results presented earlier.

B. BACKGROUND

Stiffened plates are basic structural components of many items. Metal stiffened plates can be found on bridges, buildings, automobiles, aircraft, naval vessels, and offshore platforms. In ship design, a stiffener is a metal structure composed of a web and flange. Stiffeners placed on one or both sides of a plate add strength and hinder overall collapse of the plate panel. Because of the structural complexity of stiffened plates, understanding their elastic instability is of great importance to ship designers and requires careful study.

Stiffened plate investigations occur in three general forms: theoretical, using classical and emerging theory; numerical, using finite element methods and computer-aided simulation; and experimental, using actual grillages. It is enlightening to compare the results of all three general forms of investigation. With regard to bulb-flat stiffened plates, it appears that most of what is known of their behavior comes from numerical and experimental investigations. This investigation attempts to contribute new theoretical insights into the behavior of bulb-flat stiffened plates.

The use of bulb-flat plate stiffeners in ship design is said to reduce building time and maintenance cost. Companies that produce bulb-flat plate stiffeners manufacture each stiffener as a single unit, which reportedly results in less production cost compared to welded or fabricated stiffeners. Additionally, the curved surface of the bulb-flat traps less moisture resulting in less corrosion. The shape of the bulb-flat stiffener is much easier to inspect, weld, and paint. These benefits save significant repair and maintenance costs over the lifetime of the vessel.

Advocates of bulb-flat structures applaud the advantages gained by using bulb-flats. The Jiangyin Bridge in China and the Oresund Bridge that links Denmark to Sweden are major constructions incorporating bulb-flat geometry.

C. LITERATURE SEARCH

In his bibliography, Langhaar includes a list of books and articles that well serve the reader interested in general developments and special topics in mechanics. Notable is the history and theory of plate stability discussed thoroughly in Bleich [1], who acknowledges G.H. Bryan as the originator of the study of plate stability under edge

compression. Bleich's discussion on rectangular plates under uniform axial compression and stiffened plates under axial compression are applicable to this investigation. His demonstration on the theory of buckling of centrally loaded columns by torsion and flexure serves as a fundamental basis for the buckling analysis in Chapter III.

A series of papers by Chou and Chapman [3] are noteworthy because they address the buckling behavior of bulb-flat stiffened plates. Their study presents an improved design method, iterative in nature, for determining the buckling load of the structure against the torsional buckling of the stiffener. They validate the study using FINASIC, a finite element program, and compare the results to actual tests on cruciform struts and box columns containing bulb-flat stiffeners.

An interesting aspect of their theoretical analysis is the idealization of the bulb-flat flange as an equivalent angle flange. That is, they treat the bulb-flat cross-section like a rectangular cross-section in regards to the bulb-flat torsional and warping properties. Chapter II addresses this treatment and shows that idealization imputes error in the calculation of the bulb-flat cross-section's torsional rigidity. Developing and using expressions that maintain the bulb-flat geometry yields more accurate cross-sectional property data resulting in a more accurate analysis.

Other work relevant to this investigation includes research and a series of papers by Danielson et al. [5, 6, 7, 8, and 9] analyzing the tripping of a beam attached to a plate under lateral pressure loading. His investigation includes the assumption that the stiffener behaves like a thin-walled open section beam. Applying nonlinear beam theory, he obtains an analytic expression for the buckling of stiffened plate structures under longitudinal compression. His work includes investigations of the buckling load of ship grillages under axial compression with and without lateral pressure [14 and 15]. He uses finite element based eigenvalue analysis to gain insight into the ways the buckling loads and modes vary given the grillage dimensions. In new unpublished work, he extends his previous work by re-deriving buckling load formulas that incorporate different assumptions about buckling behavior.

D. NOTATION AND CONVENTIONS

A_f	Area of the flange
A_s	$A_f + A_w$, Area of the stiffener
A_w	Area of the web
D	$\frac{Eh^3}{12\left(1-\nu^2\right)}$, Bending stiffness coefficient
E	Modulus of elasticity of the material (force/length^2)
G	$\frac{E}{2\left(1+\nu\right)}$, Shear modulus, modulus of rigidity
I_{xx}, I_{yy}, I_c	Moments of inertia about the axes and centroid in (x, y) coordinate system (length^4)
I_{xy}	Product of inertia about the origin in (x, y) coordinate system (length^4)
I_{xc}, I_{yc}	Moments parallel to the axes through the centroid in (x, y) coordinate system (length^4)
I_{xyc}	Product of inertia about the centroid in (x, y) coordinate system (length^4)
M_x, M_y	Bending moments (force/length) or first moments (length^3)
R	Region defined by the cross-section of the flange (length^2)
h_f	Height of flange (length)
h_w	Height of the web (length)
h_s	$h_w + h_f$, Height of the stiffener (length)
m	Slope of a line or line segment
r, r_1	Radius of curvature (length)
t_{bf}	Thickness of the flange bulb (length)
t_f	$t_w + t_{bf}$, Maximum thickness of flange (length)

t_p	Thickness of plate (length)
t_w	Thickness of the web (length)
x, y	Bulb-flat flange coordinate system
x_c, y_c	Bulb-flat flange coordinate system where the centroid coincides with the origin of the coordinate system
x_1, x_2, x_3	Plate structure coordinate system
α, θ	Angle (radians)
ν	Poisson's ratio
σ	Normal stress (force/length^2)

THIS PAGE INTENTIONALLY LEFT BLANK

II. BULB-FLAT FLANGE CROSS-SECTION PROPERTIES

A. INTRODUCTION

A wealth of knowledge exists on the behavior of stiffeners with common geometries such as I, T, Z, angle, channel, and flat-bar cross-sections. These common geometries possess certain cross-sectional properties that are relatively easy to derive. Studying uncommon cross-sections, such as the bulb-flat cross-section, is often difficult because obtaining the section properties of such cross-sections requires considerably more effort.

This chapter presents expressions to determine the planar properties of the bulb-flat cross-section. Subsequent analysis of the stiffened plate structure requires knowledge of the planar property values for a specified cross-section.

B. CROSS-SECTIONAL BOUNDARY AND PLANAR PROPERTIES

Consider the cross-section of a bulb-flat that extends to one side of the web as shown in Figures 1-3. Figure 1 shows the entire stiffener cross-section composed of the bulb-flat flange and thin web. Figure 2 and Figure 3 show only the flange horizontally oriented. Five independent variables (t_w, t_{bf}, r, r_1, and α) uniquely determine the flange boundary. Using both Figure 2 and Figure 3, the following labeling is established. The variable t_w denotes the web thickness defined by the vertical distance between point 4 and point 5. The variable t_{bf} denotes the bulb thickness defined by the vertical distance between point 9 and a point horizontal to point 5. The total flange thickness (at its maximum value) is denoted by $t_f = t_w + t_{bf}$ defined by the vertical distance between point 9 and the line formed by points 3 and 4. The corners of the cross-section have radii of curvature r and r_1. Points 5-6-7 and 8-9-10 define the corners with radius of curvature r. Points 1-2-3 define the corner with radius r_1. The cross-section has a flat portion defined by the points 7 and 8, that slopes α degrees from the y-axis.

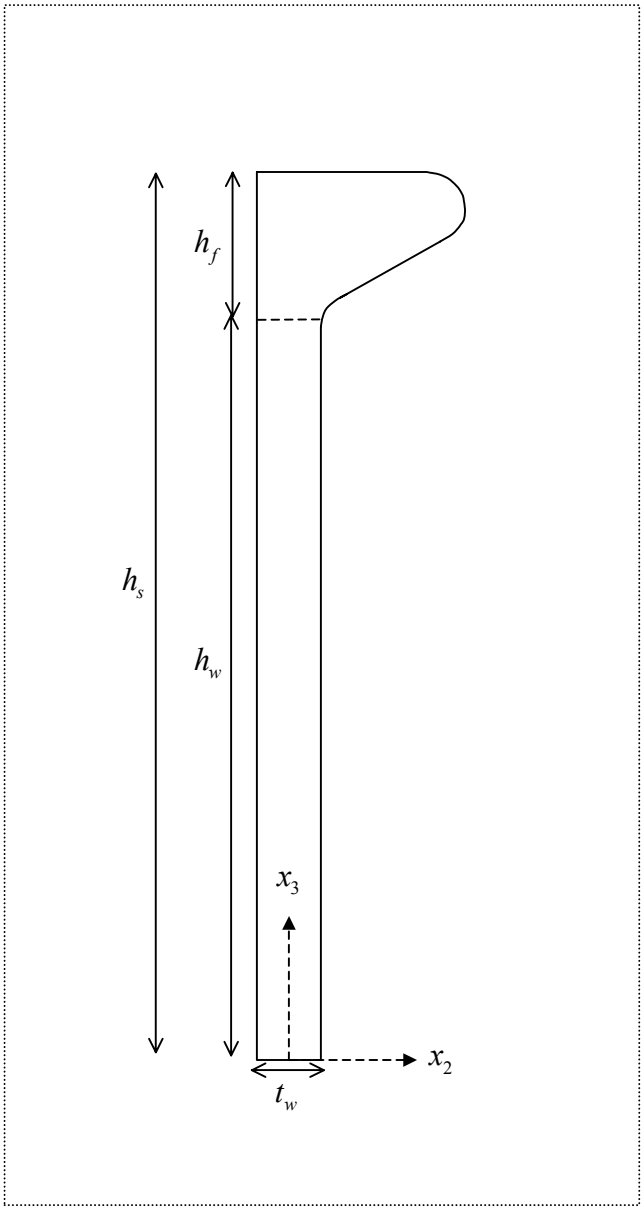

Figure 1 Bulb-flat stiffener cross-section

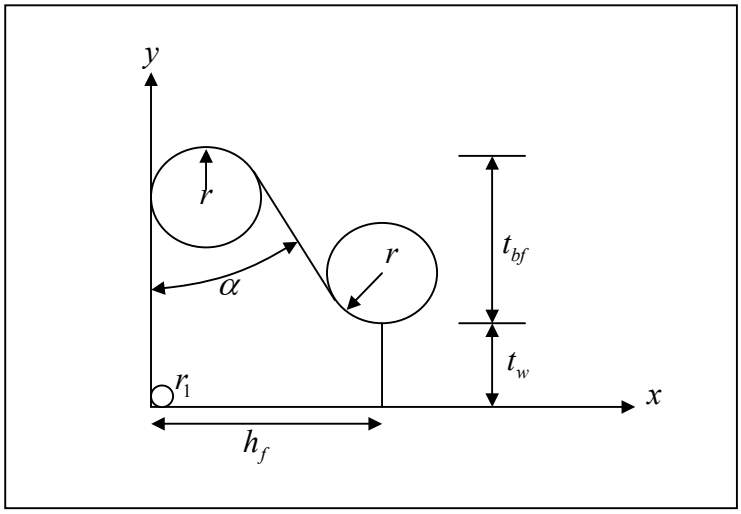

Figure 2 Bulb-flat flange geometry

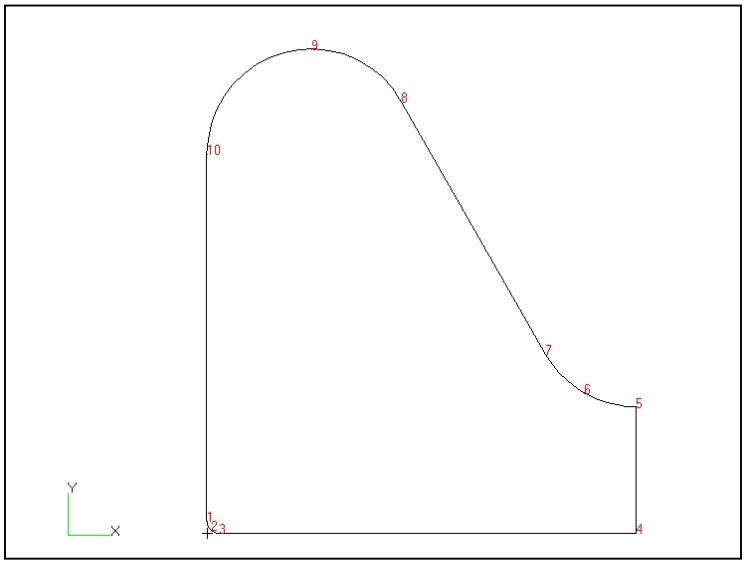

Figure 3 MSC Patran picture of bulb-flat flange boundary points for cross-section properties

Let h_f denote the flange height. The boundary of the flange includes two vertical sides $x = 0$ and $x = h_f$, where

$$h_f = t_{bf} \tan\alpha + r\left(1 - 2\tan\alpha + 2\sec\alpha\right) \tag{1}$$

and $0 < \alpha < \pi/2$ [1] (see Appendix A). The upper and lower boundaries of the cross-section are defined by the following functions. The upper boundary of the flange cross-section is given by:

$$f(x) = \begin{cases} f_1(x) = \left(t_w + t_{bf} - r\right) + \sqrt{r^2 - \left(x - r\right)^2}, & 0 \le x < r + r\cos\alpha \\ f_2(x) = -x\cot\alpha + t_w + t_{bf} + r\left(\cot\alpha + \csc\alpha - 1\right), & r + r\cos\alpha \le x < h_f - r\cos\alpha \\ f_3(x) = \left(t_w + r\right) - \sqrt{r^2 - \left(x - h_f\right)^2}, & h_f - r\cos\alpha \le x \le h_f \end{cases} \tag{2}$$

The lower boundary of the flange cross-section is given by:

$$g(x) = \begin{cases} g_1(x) = r_1 - \sqrt{r_1^2 - \left(x - r_1\right)^2}, & 0 \le x < r_1 \\ g_2(x) = 0, & r_1 \le x \le h_f \end{cases} \tag{3}$$

Given the upper, lower, and vertical boundaries, the cross-section of the flange is the bounded region R defined by $0 \le x \le h_f$, $g(x) \le y \le f(x)$, with $f(x)$ and $g(x)$ on $x \in \left[0, h_f\right]$. The flange cross-sectional planar properties can be calculated from the following integral expression where m, n are nonnegative integers (see Appendix B for details of the integral derivation):

$$\iint_R x^m y^n \, dA = \int_0^{h_f} \int_{g(x)}^{f(x)} x^m y^n \, dy \, dx = \frac{1}{n+1} \int_0^{h_f} x^m \left\{ \left[f(x) \right]^{n+1} - \left[g(x) \right]^{n+1} \right\} dx \tag{4}$$

Substitution of expressions (2) and (3) into expression (4) yields

[1] As $\alpha \to 0$, the flange geometry resembles an angle flange with a rounded end of radius r whose cross-section properties could be approximated with an equivalent rectangle.

$$
\begin{aligned}
\iint_R x^m y^n dA = {} & \frac{1}{n+1} \int_{-\frac{\pi}{2}}^{\frac{\pi}{2}-\alpha} \left(r + r\sin\theta\right)^m \left(t_w + t_{bf} - r + r\cos\theta\right)^{n+1} r\cos\theta \, d\theta \\
& + \frac{1}{n+1} \int_{r+r\cos\alpha}^{h_f - r\cos\alpha} x^m \left(-x\cot\alpha + t_w + t_{bf} + r\cot\alpha + r\csc\alpha - r\right)^{n+1} dx \\
& + \frac{1}{n+1} \int_{\alpha-\frac{\pi}{2}}^{0} \left(h_f + r\sin\theta\right)^m \left(t_w + r - r\cos\theta\right)^{n+1} r\cos\theta \, d\theta \\
& - \frac{1}{n+1} r_1^{m+n+2} \int_{-\frac{\pi}{2}}^{0} \left(1+\sin\theta\right)^m \left(1-\cos\theta\right)^{n+1} \cos\theta \, d\theta
\end{aligned}
\tag{5}
$$

where

$$
h_f = t_{bf}\tan\alpha + r\left(1 - 2\tan\alpha + 2\sec\alpha\right)
$$

$$
0 < \alpha < \frac{\pi}{2}, \quad -\frac{\pi}{2} \le \theta \le \frac{\pi}{2}, \quad 0 \le x \le h_f
$$

Throughout this investigation, the planar property values for the bulb-flat flange are calculated using integral expression (5). Appendix B contains a summary of the planar property formulas. For brevity, the expansion of each general planar property formula is omitted.

Integral expression (5) can be specialized for a class of bulb-flat flange cross-sections by assigning a value to one or more of the variables. For example, by setting $\alpha = \pi/6$, integral expression (5) defines planar property formulas for a class of bulb-flat cross-sections with a 30^o slope. Additionally, if the radius of curvature of the cross-section corner r_1 is assumed to be one-tenth of the web thickness t_w $\left(r_1 = t_w/10\right)$, the integral defines planar property formulas for a specific type of the 30^o slope cross-sections. In this case, terms involving r_1 become negligible for this particular class of flange cross-sections. Cross-sectional planar property values for this special class can be calculated from the following integral expression (6) where m, n are nonnegative integers, $\alpha = \pi/6$, and the term involving r_1 is neglected:

$$\iint_R x^m y^n dA = \frac{1}{n+1}\int_{-\frac{\pi}{2}}^{\frac{\pi}{3}} \left(r + r\sin\theta\right)^m \left(t_w + t_{bf} - r + r\cos\theta\right)^{n+1} r\cos\theta\, d\theta$$

$$+\frac{1}{n+1}\int_{r\left(1+\frac{\sqrt{3}}{2}\right)}^{t_{bf}\frac{\sqrt{3}}{3}+r\left(1+\frac{\sqrt{3}}{6}\right)} x^m \left(-x\sqrt{3} + t_w + t_{bf} + r\left(1+\sqrt{3}\right)\right)^{n+1} dx \qquad (6)$$

$$+\frac{1}{n+1}\int_{-\frac{\pi}{3}}^{0} \left(h_f + r\sin\theta\right)^m \left(t_w + r - r\cos\theta\right)^{n+1} r\cos\theta\, d\theta$$

where

$$h_f = t_{bf}\frac{\sqrt{3}}{3} + r\left(1+\frac{2\sqrt{3}}{3}\right)$$

$$-\frac{\pi}{2} \le \theta \le \frac{\pi}{2}, \quad 0 \le x \le h_f$$

The following formulas are algebraic expansions of expression (6) for the specialized class of bulb-flat flanges. The flange area and centroid formulas are

$$A_f = -\left(1-\frac{\pi}{4}\right)r^2 + \left[\left(1+\frac{2\sqrt{3}}{3}\right)t_w + \left(1+\frac{\sqrt{3}}{3}\right)t_{bf}\right]r + \frac{\sqrt{3}}{6}{t_{bf}}^2 + \frac{\sqrt{3}}{3}t_w t_{bf}$$

$$\bar{x} = \left[\begin{array}{l}\left(\frac{\pi}{4} - \frac{\pi\sqrt{3}}{9} - \frac{2}{9}\right)r^3 + \left(\frac{7}{6} + \frac{2\sqrt{3}}{3}\right)r^2 t_w + \left(1 + \frac{\sqrt{3}}{3} - \frac{\pi\sqrt{3}}{18}\right)r^2 t_{bf} \\ + \left(\frac{2+\sqrt{3}}{3}\right)r t_w t_{bf} + \left(\frac{1+\sqrt{3}}{6}\right)r{t_{bf}}^2 + \frac{1}{6}t_w{t_{bf}}^2 + \frac{1}{18}{t_{bf}}^3\end{array}\right]\frac{1}{A_f}$$

$$\bar{y} = \left[\begin{array}{l}\left(\frac{11\sqrt{3}}{18} - \frac{7\pi}{12} + \frac{5}{6}\right)r^3 + \left(\frac{\pi}{4} - 1\right)r^2 t_w + \left(\frac{5\pi}{12} - 1 - \frac{\sqrt{3}}{3}\right)r^2 t_{bf} \\ + \left(\frac{1}{2} + \frac{\sqrt{3}}{3}\right)r{t_w}^2 + \left(1 + \frac{\sqrt{3}}{3}\right)r t_w t_{bf} + \left(\frac{1}{2} + \frac{\sqrt{3}}{6}\right)r{t_{bf}}^2 \\ + \frac{\sqrt{3}}{6}{t_w}^2 t_{bf} + \frac{\sqrt{3}}{6}t_w{t_{bf}}^2 + \frac{\sqrt{3}}{18}{t_{bf}}^3\end{array}\right]\frac{1}{A_f}$$

Formulas for the moments of the specialized class of flanges are

$$I_{xx} = \left(-1+\frac{5\pi}{16}\right)r^4 + \left[\left(\frac{5}{3}+\frac{11\sqrt{3}}{9}-\frac{7\pi}{6}\right)t_w + \left(\frac{11\sqrt{3}}{18}+\frac{5}{3}-\frac{5\pi}{6}\right)t_{bf}\right]r^3$$
$$+\left[\left(-1+\frac{\pi}{4}\right){t_w}^2 + \left(-\frac{2\sqrt{3}}{3}-2+\frac{5\pi}{6}\right)t_w t_{bf} + \left(-1+\frac{5\pi}{12}-\frac{\sqrt{3}}{3}\right){t_{bf}}^2\right]r^2$$
$$+\left[\left(\frac{2\sqrt{3}}{9}+\frac{1}{3}\right){t_w}^3 + \left(\frac{\sqrt{3}}{3}+1\right)\left({t_w}^2 t_{bf} + t_w {t_{bf}}^2\right) + \left(\frac{\sqrt{3}}{9}+\frac{1}{3}\right){t_{bf}}^3\right]r$$
$$+\frac{\sqrt{3}}{36}{t_{bf}}^4 + \frac{\sqrt{3}}{6}{t_w}^2{t_{bf}}^2 + \frac{\sqrt{3}}{9}t_w{t_{bf}}^3 + \frac{\sqrt{3}}{9}{t_w}^3 t_{bf}$$

$$I_{yy} = \left(\frac{11\sqrt{3}}{27}-\frac{2\pi\sqrt{3}}{9}+\frac{2}{9}+\frac{13\pi}{144}\right)r^4 + \left[\left(\frac{26\sqrt{3}}{27}+\frac{5}{3}\right)t_w + \left(\frac{43\sqrt{3}}{54}+\frac{4}{3}-\frac{2+\sqrt{3}}{9}\pi\right)t_{bf}\right]r^3$$
$$+\left[\left(\frac{7\sqrt{3}}{9}+\frac{4}{3}\right)t_w t_{bf} + \left(\frac{1+\sqrt{3}}{3}-\frac{\pi}{18}\right){t_{bf}}^2\right]r^2 + \left[\left(\frac{2\sqrt{3}}{9}+\frac{1}{3}\right)t_w{t_{bf}}^2 + \left(\frac{\sqrt{3}}{27}+\frac{1}{9}\right){t_{bf}}^3\right]r$$
$$+\frac{\sqrt{3}}{27}t_w{t_{bf}}^3 + \frac{\sqrt{3}}{108}{t_{bf}}^4$$

$$I_c = I_{xx} + I_{yy} - A_f\left(\bar{x}^2 + \bar{y}^2\right)$$

C. TORSIONAL RIGIDITY

The torsion of a beam is the application of twisting moments at both ends of the beam. In the absence of side surface tractions and if the ends of the bar are free to warp, the beam experiences pure torsion. The Saint-Venant constant for uniform torsion or torsional constant J is the ratio of an applied beam twisting moment M_t to the product of the shear modulus (modulus of rigidity) G and the beam twist per unit length θ.

$$J = \frac{M_t}{G\theta} \tag{7}$$

The role of the quantity GJ (torsional rigidity) in the twisting of a beam is similar to the role of the quantity EI (flexural rigidity) in the bending of a beam.

1. Exact Value Using the Stress Function Method

One method of determining the torsional rigidity of a cross-section (solving the torsion problem) is by finding the stress function[2]. Analysis of torsional behavior requires finding the stress function Φ, which is an exact solution to Poisson's equation:

$$\begin{aligned} &\nabla^2\Phi = \frac{\partial^2\Phi}{\partial x^2} + \frac{\partial^2\Phi}{\partial y^2} = -2G\theta \text{ in } R \\ &\Phi = 0 \text{ on the boundary of } R \end{aligned} \tag{8}$$

Donaldson [10, p. 376] shows the torsional constant as

$$J = -\frac{4}{\nabla^2\Phi}\iint_R \Phi dA \tag{9}$$

The following example illustrates using the stress function method to determine the torsional constant. Let the boundary of an elliptic cross-section with the origin coinciding with the centroid be given by

$$\frac{x^2}{a^2} + \frac{y^2}{b^2} - 1 = 0 \tag{10}$$

which has area and inertia properties

$$A = \pi ab \quad I_c = \frac{1}{4}\pi ab\left(a^2 + b^2\right)$$

Take the stress function in the form

$$\Phi = c\left(\frac{x^2}{a^2} + \frac{y^2}{b^2} - 1\right) \tag{11}$$

where c is a constant. Hence,

$$\nabla^2\Phi = 2c\left(\frac{1}{a^2} + \frac{1}{b^2}\right) = 2c\frac{a^2 + b^2}{a^2b^2} = -2G\theta \tag{12}$$

After solving for c, equation (11) satisfies the conditions of (8) and is zero on the boundary of the region when

[2] Introduced by Ludwig Prandtl.

$$c = -G\theta \frac{a^2 b^2}{a^2 + b^2}$$

Therefore

$$\begin{aligned} J &= -\frac{4}{\nabla^2 \Phi} \iint_A \Phi dA \\ &= -\frac{4}{2c\left(\frac{1}{a^2} + \frac{1}{b^2}\right)} \iint_A c\left(\frac{x^2}{a^2} + \frac{y^2}{b^2} - 1\right) dA \\ &= -\frac{2}{\left(\frac{1}{a^2} + \frac{1}{b^2}\right)} \left[\frac{1}{a^2}\left(\frac{1}{4}\pi a^3 b\right) + \frac{1}{b^2}\left(\frac{1}{4}\pi a b^3\right) - \pi ab\right] \\ &= -\frac{2a^2 b^2}{a^2 + b^2}\left[\frac{1}{4}\pi ab + \frac{1}{4}\pi ab - \pi ab\right] = \frac{\pi a^3 b^3}{a^2 + b^2} \end{aligned} \tag{13}$$

When $a = b$, the results correspond with the known formula $J = \pi a^4 / 2$ for the circular cross-section.

The torsion problem has been solved exactly for other common cross-sectional forms such as the square, rectangle, and equilateral triangle. The torsional constant can be obtained relatively easily for flanges with cross-sections that are symmetric about at least one axis. For flanges with arbitrary cross-sections, finding the exact solution is quite difficult. The reason for this is, as Donaldson [10, p. 386] notes,

> It is not difficult to write expressions that satisfy the governing differential equation, and it is not difficult to write expressions that satisfy the boundary conditions. What is difficult is to do both simultaneously.

The uncommon shape and nonsymmetrical cross-section of the bulb-flat flange make it difficult to find a stress function that satisfies simultaneously both conditions of (8). Several methods exist that attempt to simplify the search for the stress function of "difficult" cross-sections.[3] For an arbitrary cross-section, the general solution of the torsion problem is found using conformal mapping by mapping the region upon the interior and boundary of a circle, then solving the problems of Dirichlet and Neumann for

[3] Methods are generally included in references that discuss solutions to Poisson's equation or the torsion problem. Solving Poisson's equation using conformal mapping is discussed in Henrici [11, pp. 372-377].

the circular region. Approximation methods offer alternatives to solving Poisson's equation directly for the bulb-flat flange cross-section.

2. Approximate Expressions: Lower and Upper Bounds

Washizu [24] uses variational methods and includes a computational technique for obtaining accurate lower and upper bounds for torsional rigidity. His method applies the principles of minimum potential and complementary energy. Stakgold [20, pp. 579-583] presents a similar approach where he derives

$$\frac{4\left(\iint_R w\,dx\,dy\right)^2}{\iint_R \left(w_x^{\,2}+w_y^{\,2}\right)dx\,dy} \le J \le \iint_R \left(v_x^{\,2}+v_y^{\,2}\right)dx\,dy \tag{14}$$

where w vanishes on the boundary of the region and v satisfies

$$\frac{\partial^2 v}{\partial x^2}+\frac{\partial^2 v}{\partial y^2}=-2 \tag{15}$$

on the cross-sectional region. The upper bound is smallest if the region's centroid coincides with the origin. Stakgold further shows that the bounds can be improved by adding certain harmonic functions to v. It should be noted that the calculations required to apply this method to uncommon cross-sections is quite involved.

The follow examples illustrate establishing bounds using (14) and (15). To establish a lower bound for the circular cross-section, let w be the following function that vanishes on the circular boundary of radius r whose center coincides with the origin.

$$w(x,y)=x^2+y^2-r^2 \tag{16}$$

A lower bound is

$$\frac{4\left(\iint\limits_{R_{circle}} w\,dx\,dy\right)^2}{\iint\limits_{R_{circle}} \left(w_x{}^2 + w_y{}^2\right) dx\,dy} = \frac{4\left(\iint\limits_{R_{circle}} x^2 + y^2 - r^2\,dx\,dy\right)^2}{\iint\limits_{R_{circle}} 4x^2 + 4y^2\,dx\,dy}$$

$$= \frac{\left(I - Ar^2\right)^2}{I} = \frac{\left(\frac{\pi r^4}{2} - \pi r^4\right)^2}{\frac{\pi r^4}{2}} = \frac{\pi r^4}{2} = I$$

For an upper bound, let

$$v(x,y) = -\frac{1}{2}\left(x^2 + y^2\right) \tag{17}$$

that satisfies condition (15). An upper bound is

$$\iint\limits_{R_{circle}} \left(v_x{}^2 + v_y{}^2\right) dx\,dy = \iint\limits_{R_{circle}} \left(x^2 + y^2\right) dx\,dy = I$$

The lower and upper bounds confirm the fact that for any circular cross-section, $I \le J \le I$ or $J = I$; that is, the torsional constant equals the moment of inertia about the centroid.

For the square cross-section, with sides of length $2a$, establish a lower bound by choosing w to be the following function, which vanishes on the boundary centered on the origin:

$$w(x,y) = (x+a)(x-a)(y+a)(y-a) = \left(x^2 - a^2\right)\left(y^2 - a^2\right) \tag{18}$$

A lower bound is

$$\frac{4\left(\int\limits_{-a}^{a}\int\limits_{-a}^{a} w\,dx\,dy\right)^2}{\int\limits_{-a}^{a}\int\limits_{-a}^{a} \left(w_x{}^2 + w_y{}^2\right) dx\,dy} = \frac{4\left(\frac{16a^6}{9}\right)^2}{\frac{256a^8}{45}} = \frac{20a^4}{9} = 2.222\overline{2}a^4 \tag{19}$$

An upper bound is established by letting v be the same as equation (17).

$$\int_{-a}^{a}\int_{-a}^{a}\left(v_x{}^2+v_y{}^2\right)dx\,dy=\int_{-a}^{a}\int_{-a}^{a}\left(x^2+y^2\right)dx\,dy=\frac{8a^4}{3}=2.666\overline{6}a^4 \tag{20}$$

Combining expressions (19) and (20), establishes the following lower and upper bounds for the torsional constant of a square cross-section:

$$2.222\overline{2}a^4\le J\le 2.666\overline{6}a^4 \tag{21}$$

The exact value of the torsional constant for a square cross-section is $J=2.2496a^4$, as shown later.

Application of the lower and upper bounds method to the bulb-flat flange cross-section involves rather arduous calculations. Because the upper bound is smallest if the region's centroid coincides with the origin, the boundary equations (2) and (3) must be modified so that the centroid and origin coincide. Let the flange cross-section defined by equations (2) and (3) be modified for the bounded region R_c (the subscribe c indicating the centroid coincides with the origin) defined by $-\overline{x}\le x_c\le h_f-\overline{x}$, $g(x_c)\le y_c\le f(x_c)$, with $f(x_c)$ and $g(x)_c$ on $x_c\in\left[-\overline{x},h_f-\overline{x}\right]$. A function w that vanishes on R_c is

$$\begin{aligned}w(x_c,y_c)=&\left[y_c-f_1(x_c)\right]\left[y_c-f_2(x_c)\right]\left[y_c-f_3(x_c)\right]\times\\&\left[y_c-g_1(x_c)\right]\left[y_c-g_2(x_c)\right]\left(x_c+\overline{x}\right)\left(x_c-h_f+\overline{x}\right)\end{aligned} \tag{22}$$

Using (22) in (14) results in very complicated expressions and provides only modest gains to establishing accurate bounds for the bulb-flat flange torsional constant. Other approximation methods may provide simpler means to obtain the torsional constant for the bulb-flat flange cross-section.

3. Approximate Expressions: k*A^4/I

Saint-Venant[4] offers an approximate expression for the torsional constant of any solid section (except certain common sections):

$$J \approx \frac{1}{4\pi^2}\frac{A^4}{I_c} \tag{23}$$

where A is the cross-sectional area and I_c is the moment of inertia about the centroid. Let k be defined as

$$k = \frac{I_c J}{A^4} \tag{24}$$

for a cross-section where expressions for the area, moment of inertia about the centroid, and torsional constant are known. Consider the following table showing the results of (24) for common cross-sections.

Table 1 Saint Venant approximate expression for common cross-sections

Cross-Section	Parameter	A	I_c	J	$k = \frac{I_c J}{A^4}$
Circular	r	πr^2	$\frac{1}{2}\pi r^4$	$\frac{1}{2}\pi r^4$	$\frac{\pi^2 r^8}{4\pi^4 r^8} = \frac{1}{4\pi^2} \approx 0.02533$
Elliptic	a, b	πab	$\frac{1}{4}\pi ab\left(a^2+b^2\right)$	$\frac{\pi a^3 b^3}{a^2+b^2}$	$\frac{\pi^2 a^4 b^4}{4\pi^4 a^4 b^4} = \frac{1}{4\pi^2} \approx 0.02533$
Square	$2a$	$4a^2$	$\frac{8}{3}a^4$	$2.2496a^4$	$0.0234\overline{3}$

For the given cross-sections, the value of k is a fixed constant that does not depend on the parameters of the cross-section.

In other cross-sections, the value of k may vary as the parameters that define the cross-section vary. For rectangular cross-sections with length $2b$ and thickness $2t$, k

[4] Discussed by Saint-Venant, "Sur une formule donnant approximativement le moment de torsion", *Comptes Rendus,* vol. 88, 1879, pp. 142-154, and in Timoshenko and Goodier [22, pp. 301-302].

varies for different values of the ratio t/b.[5] In those cases, the torsional constant can be obtained from

$$J = \frac{1}{3}(2b)(2t)^3\left(1-\frac{192t}{\pi^5 b}\sum_{n=1,3,5,\ldots}^{\infty}\frac{1}{n^5}\tanh\frac{n\pi b}{2t}\right) \tag{25}$$

developed in Timoshenko and Goodier [22, pp. 309-313]. For a square cross-section, (25) yields the J expression shown for the square cross-section in Table 1. For rectangular cross-sections with parameters $2t$ and $2b$, the area and inertia properties are

$$A = 4bt \quad I_c = \frac{4}{3}bt\left(b^2+t^2\right)$$

The expression for k is thus

$$k = \frac{I_c J}{A^4} = \frac{1}{36}\left(1+\frac{t^2}{b^2}\right)\left(1-\frac{192t}{\pi^5 b}\sum_{n=1,3,5,\ldots}^{\infty}\frac{1}{n^5}\tanh\frac{n\pi b}{2t}\right)$$

Pilkey and Chang [18, p. 103] express the torsional constant formula for rectangular cross-sections as

$$J \approx \frac{1}{3}(2b)(2t)^3(1-0.63\frac{t}{b}+0.052\frac{t^5}{b^5}), \quad \text{where} \quad t \le b \tag{26}$$

which is a simplification of (25). Expression (26) gives adequate accuracy and is used in the analysis presented in later sections. For elongated rectangular cross-sections, the torsional constant can be obtained from

$$J \approx \frac{1}{3}(2b)(2t)^3 \quad \text{where} \quad t \ll b \tag{27}$$

As the ratio t/b approaches zero, then (26) approaches (27).

[5] This effect can be deduced from discussions found in Timoshenko and Goodier [22, pp. 309-313], in Donaldson [10, pp.390-394], or in Oden [16, p. 44].

It would be useful to identify classes or sub-classes of bulb-flat cross-sections possessing a fixed constant k. Corus Group[6] provides a special profile brochure [4] that contains technical data on 59 bulb-flat cross-sections commonly requested. The following tables (Table 2 and Table 3) reflect all 59 bulb-flat cross-sections published in the brochure. The cross-sections represent a class of bulb-flat flanges where $\alpha = \pi / 6$ and the values for t_w, t_{bf}, and r are as given in the tables. The brochure states a tolerance level for the value of r_1. For ease of calculations, it is assumed that $r_1 = t_w / 10$, which obeys the tolerance level stated in the brochure.

[6] Corus Group was formed in 1999 through the merger of British Steel and Koninklijke Hoogovens. The company is a leading international metal company and one of the world's leading producers of bulb-flat profiled metals.

Table 2 Finite element results for bulb-flat flange cross-sections

Variables t_w, t_{bf}, and r, are given, while $r_1 = (1/10)t_w$ and $\alpha = \pi/6$ radians.							
Model	t_w	t_{bf}	r	A_f	I_c	J	k
	mm	mm	mm	mm^2	mm^4	mm^4	
1	6.0	17.0	5.0	335.59	21903	13339	0.023035
2	7.0	17.0	5.0	356.15	24609	15065	0.023043
3	8.0	17.0	5.0	376.70	27480	16915	0.023084
4	6.5	19.0	5.5	410.79	32907	19936	0.023038
5	7.0	19.0	5.5	422.19	34720	21076	0.023032
6	8.0	19.0	5.5	444.97	38492	23475	0.023049
7	10.0	19.0	5.5	490.54	46667	28716	0.023144
8	7.0	22.0	6.0	519.50	53120	31583	0.023034
9	8.0	22.0	6.0	545.10	58392	34823	0.023031
10	9.0	22.0	6.0	570.69	63911	38262	0.023054
11	11.5	22.0	6.0	634.66	78896	47656	0.023175
12	8.0	25.0	7.0	681.93	91182	54641	0.023039
13	9.0	25.0	7.0	711.41	99088	59532	0.023030
14	10.0	25.0	7.0	740.89	107316	64696	0.023042
15	11.5	25.0	7.0	785.09	120303	72912	0.023088
16	8.5	28.0	8.0	849.67	141249	85076	0.023056
17	9.0	28.0	8.0	866.36	146751	88465	0.023045
18	10.0	28.0	8.0	899.72	158047	95505	0.023035
19	11.0	28.0	8.0	933.08	169751	102873	0.023038
20	12.0	28.0	8.0	966.43	181882	110576	0.023055
21	9.0	31.0	9.0	1035.54	209455	126681	0.023075
22	10.0	31.0	9.0	1072.79	224516	135976	0.023049
23	11.0	31.0	9.0	1110.03	240055	145706	0.023038
24	12.0	31.0	9.0	1147.27	256095	155831	0.023035
25	9.5	34.0	10.0	1239.52	299704	181896	0.023095
26	10.0	34.0	10.0	1260.02	309570	187930	0.023076
27	11.0	34.0	10.0	1301.21	329720	200430	0.023052
28	12.0	34.0	10.0	1342.34	350449	213450	0.023039
29	10.0	37.0	11.0	1461.61	416284	253399	0.023114
30	11.0	37.0	11.0	1506.63	441894	269103	0.023079

Table 3 Finite element results for bulb-flat flange cross-sections (cont)

Variables t_w, t_{bf}, and r, are given, while $r_1 = (1/10)t_w$ and $\alpha = \pi/6$ radians.							
Model	t_w	t_{bf}	r	A_f	I_c	J	k
31	12.0	37.0	11.0	1551.64	468166	285438	0.023054
32	10.5	40.0	12.0	1701.82	563855	344119	0.023133
33	11.0	40.0	12.0	1726.27	579944	353915	0.023113
34	12.0	40.0	12.0	1775.17	612687	374094	0.023081
35	13.0	40.0	12.0	1824.07	646209	395021	0.023058
36	11.0	43.0	13.0	1960.15	747463	457230	0.023151
37	12.0	43.0	13.0	2012.93	787681	481743	0.023113
38	13.0	43.0	13.0	2065.72	828771	507140	0.023082
39	11.5	46.0	14.0	2236.59	972529	596102	0.023167
40	12.0	46.0	14.0	2264.93	997033	610924	0.023146
41	13.0	46.0	14.0	2321.60	1046772	641379	0.023111
42	14.0	46.0	14.0	2378.26	1097519	672871	0.023084
43	12.0	49.0	15.0	2531.15	1244856	764377	0.023182
44	13.0	49.0	15.0	2591.71	1304401	800436	0.023142
45	14.0	49.0	15.0	2652.26	1365058	837738	0.023110
46	15.0	49.0	15.0	2712.81	1426867	876255	0.023085
47	12.5	53.5	16.5	2990.36	1736393	1069001	0.023213
48	13.0	53.5	16.5	3023.55	1774843	1092092	0.023193
49	14.0	53.5	16.5	3089.94	1852703	1139236	0.023154
50	15.0	53.5	16.5	3156.31	1931884	1187887	0.023123
51	16.0	53.5	16.5	3222.69	2012431	1237937	0.023097
52	13.0	58.0	18.0	3487.42	2360220	1456675	0.023243
53	14.0	58.0	18.0	3559.63	2458317	1515332	0.023202
54	15.0	58.0	18.0	3631.84	2557909	1575695	0.023166
55	16.0	58.0	18.0	3704.05	2659049	1637762	0.023135
56	14.0	62.5	19.5	4061.35	3199092	1977224	0.023249
57	15.0	62.5	19.5	4139.39	3322389	2050964	0.023209
58	17.0	62.5	19.5	4295.45	3574247	2204506	0.023145
59	20.0	62.5	19.5	4529.52	3966020	2449749	0.023082
						Mean Value	0.023099
						Standard Deviation	5.95E-5
						Median Value	0.023084

From Table 2 and Table 3, values for k appear "nearly" fixed for the specified class of bulb-flat flange cross-sections. When applied to the bulb-flat flange cross-section, the Saint Venant approximation (23) with $k = 1/4\pi^2 \approx 0.0253$ generates torsion values that are 9% to 10% larger than values obtained from finite element methods. However, based on the above tables, the following approximate expression yields reasonably accurate values for the torsional constant of flanges within the specified class when compared to finite element data.

$$J_f \approx 0.0231 \frac{{A_f}^4}{I_c} \tag{28}$$

Hence, expression (28) serves as a working formula that approximates the torsional constant for the bulb-flange cross-sections within the specified class and is used throughout the remainder of this investigation.

4. Idealization

Success in determining the exact expression of Saint Venant's torsional constant is limited to simple cross-sections. It is common practice to use known exact expressions for simple cross-sections to approximate more difficult and multiply connected cross-sections by idealization. Idealizing is attributing a cross-section, whose properties may be partially known, with the known properties of a simple cross-section. Caution is required when applying this method to idealize the bulb-flat flange as an area-equivalent angle flange. The following illustrates mathematically the need for caution.

Consider a solid circular cross-section of radius r with area and torsional properties, respectively

$$A_{\text{circle}} = \pi r^2 \quad J_{\text{circle}} = \frac{\pi r^4}{2}$$

An area-equivalent square cross-section with sides $2l$ in length has area and torsional properties, respectively

$$A_{\text{square}} = 4l^2 \quad J_{\text{square}} = 2.2496 l^4$$

Since $A_{\text{circle}} = A_{\text{square}}$, then

$$l = \frac{\sqrt{\pi}}{2} r$$

Hence,

$$J_{\text{square}} = 2.2496 l^4 = 2.2496 \left(\frac{\sqrt{\pi}}{2} r \right)^4 = \frac{2.2496 \pi}{8} \left(\frac{\pi r^4}{2} \right) \approx 0.8834 \left(J_{\text{circle}} \right)$$

This shows that idealizing a circular cross-section as an area-equivalent square cross-section reduces the Saint Venant torsional constant of the cross-section by nearly 12%.

A similar argument shows that idealizing an elliptical cross-section as an area-equivalent rectangular cross-section reduces the Saint Venant torsional constant of the cross-section when both cross-sections have high aspect ratios. The aspect ratio for a rectangle is the length to thickness ratio l/t. A high aspect ratio means the cross-section is very long compared to its thickness. The aspect ratio for an ellipse depends on the ratio of the major axis length to the minor axis length. Consider an elliptical cross-section centered on the origin with semimajor axis a and semiminor axis b having area and torsional properties

$$A_{\text{ellipse}} = \pi a b \quad J_{\text{ellipse}} = \frac{\pi a^3 b^3}{a^2 + b^2}$$

An area-equivalent rectangular cross-section of width $2l$ and thickness $2t$, assuming $t \ll l$, has area and torsional properties

$$A_{\text{rectangle}} = 4 l t \quad J_{\text{rectangle}} \approx \frac{16 l t^3}{3}$$

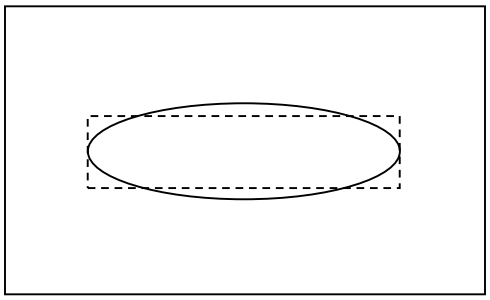

Figure 4 Idealizing an ellipse as a rectangle

As commonly done in this case, assume the two cross-sections have the same width $l = a$. Since $A_{\text{ellipse}} = A_{\text{rectangle}}$, then

$$4lt = \pi ab \Rightarrow 4at = \pi ab \Rightarrow t = \frac{\pi}{4} b$$

Hence,

$$J_{\text{rectangle}} \approx \frac{16lt^3}{3} = \frac{16a\left(\frac{\pi}{4}b\right)^3}{3} = \frac{\pi^2}{12}\left(\frac{a^2+b^2}{a^2}\right)\left(\frac{\pi a^3 b^3}{a^2+b^2}\right) = \frac{\pi^2}{12}\left(\frac{a^2+b^2}{a^2}\right) J_{\text{ellipse}}$$

The effect on the torsional constant due to the idealization depends on the relationship of the semimajor and semiminor axis lengths. As the ratio of the semiminor axis to semimajor axis approaches zero, $b/a \to 0$, then

$$\frac{\pi^2}{12}\left(\frac{a^2+b^2}{a^2}\right) \to \frac{\pi^2}{12} \approx 0.8225$$

Even though methods exist to minimize or eliminate the potential loss of torque capacity by idealization (detailed discussion omitted), the argument is that application of the idealization method requires forethought.

D. VALIDATION USING FINITE ELEMENT MODELS

Analysis of several finite element models using MSC Nastran 2001/Patran 2001-r3 software serves to validate the property formulas. The property values from formulas are compared to values from finite element models. In each finite element bulb-flat flange model, ten distinct points establish the boundary of the bulb-flat flange cross-section. Straight lines and 3-point arc curves are defined from the boundary points. A single trimmed surface is defined from the curves. The arbitrary shape option in the software's beam library is used with the maximum allowable curvature error set at 0.005. Maple 8 computer environment and a handheld calculator are used to calculate formula results. Table 4 presents planar property values for several bulb-flat flanges using expression (28), formula (76) in Appendix A, and formulas (80) - (91) in Appendix B.

The table presents a comparison of the formula values to data obtained from MSC Nastran/Patran finite element models of the cross-sections.

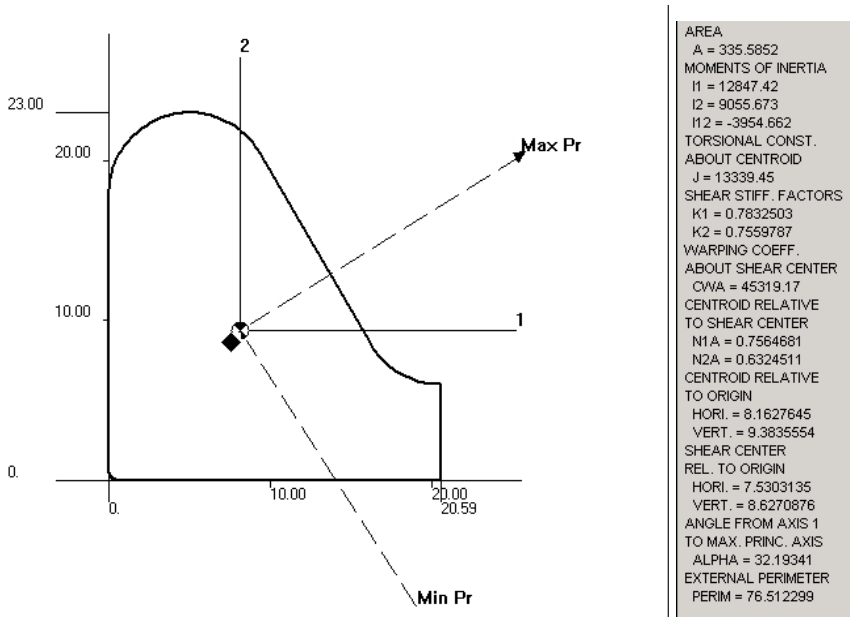

Figure 5 MSC Patran graph and data of a horizontal bulb-flat flange

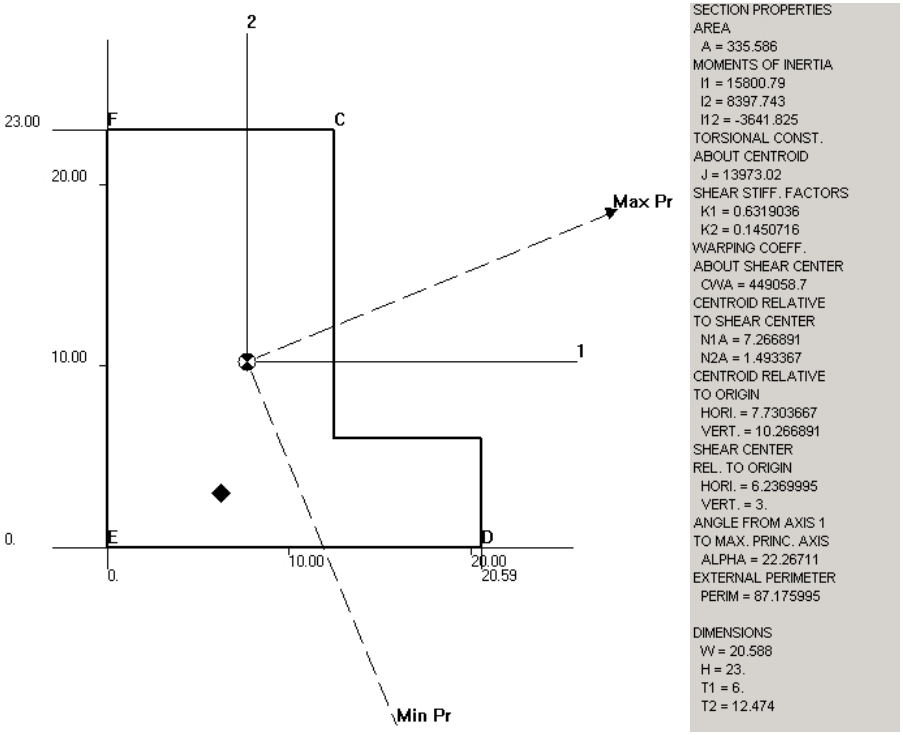

Figure 6 MSC Patran graph and data of an area-equivalent angle flange

Table 4 Comparison of flange values

Variables t_w, t_{bf}, and r, are given, while $r_1 = (1/10)t_w$ and $\alpha = \pi/6$ radians.

$$\text{Percent change} = \frac{J_f - J^{(FE)}}{J^{(FE)}} \times 100$$

* - indicates an absolute percent change of less than 0.01%.

Source	t_w	t_{bf}	r	$\bar{x}$	$\bar{y}$	A_f	I_c	**Percent change**	J_f	**Percent change**
	mm	mm	mm	mm	mm	mm^2	mm^4		mm^4	
Formula	6.0	17.0	5.0	8.163	9.384	335.59	21904	*	13376	0.28%
FE(bulb)				8.163	9.384	335.59	21903	*	13339	*
FE(angle)				7.730	10.267	335.59	24199	10.48%	13973	4.75%
Formula	8.0	17.0	5.0	8.397	10.251	376.71	27481	*	16928	0.08%
FE(bulb)				8.397	10.251	376.70	27480	*	16915	*
FE(angle)				8.010	11.035	376.71	30560	11.21%	16026	-5.26%
Formula	7.0	19.0	5.5	9.081	10.608	422.19	34722	*	21137	0.29%
FE(bulb)				9.081	10.607	422.19	34720	*	21076	*
FE(angle)				8.611	11.581	422.19	38450	10.74%	21586	2.42%
Formula	10.0	19.0	5.5	9.408	11.922	490.54	46670	*	28661	-0.19%
FE(bulb)				9.408	11.921	490.54	46667	*	28716	*
FE(angle)				9.000	12.754	490.54	52004	11.44%	26362	-8.20%
Formula	7.0	22.0	6.0	10.036	11.789	519.51	53122	*	31674	0.29%
FE(bulb)				10.036	11.789	519.50	53120	*	31583	*
FE(angle)				9.486	12.992	519.51	58776	10.65%	33449	5.91%
Formula	9.0	22.0	6.0	10.287	12.642	570.70	63914	*	38339	0.20%
FE(bulb)				10.287	12.642	570.69	63911	*	38262	*
FE(angle)				9.784	13.735	570.70	71244	11.47%	36965	-3.39%
Formula	8.0	25.0	7.0	11.574	13.429	681.94	91186	*	54785	0.26%
FE(bulb)				11.574	13.428	681.93	91182	*	54641	*
FE(angle)				10.939	14.786	681.94	100732	10.47%	58328	6.75%
Formula	10.0	25.0	7.0	11.829	14.281	740.89	107321	*	64856	0.25%
FE(bulb)				11.829	14.281	740.89	107316	*	64696	*
FE(angle)				11.243	15.528	740.90	119359	11.22%	63541	-1.79%

Examination of Table 4 reveals several noteworthy aspects. The formula results agree with the finite element results for the bulb-flat flange. The two independent sources agree almost exactly on the centroid locations $(\bar{x}, \bar{y})$, the flange area values A_f, and the values for the polar moments I_c. Though not independent, the formula values for the torsional constants J_f obtained using the approximate expression (28) differs from

the finite element values by less than one half of a percent. Such agreement supports the validation of the formula expressions.

On the other hand, note that the finite element results for the bulb-flat flange differ noticeably with the finite element results for an area-equivalent angle flange. The centroid coordinates $(\bar{x}, \bar{y})$ differ considerably. The moments I_c differ approximately 10%. Only the flange area results agree which is by design. This strengthens the case that using an angle flange as an area-equivalent to the bulb-flat flange produces error.

To determine the values for the area and torsional constant for the stiffener that includes the web and bulb-flat flange together, let the stiffener have total height h_s. The stiffener area formula is given by

$$A_s = A_f + A_w = A_f + \left(h_s - h_f\right)t_w \tag{29}$$

The membrane analogy for uniform torsion is a useful tool for visualizing the distribution of shearing stress in beam cross-sections and provides justification for approximating the torsional constant of the stiffener. If a membrane of constant thickness were stretched over a beam cross-section, fixed against the boundary of the cross-section, and filled with a gas exerting normal pressure on the membrane surface, the volume under the membrane is proportional to the torque-carrying capacity of the cross-section. Additionally, the torque-carrying capacity of a cross-section composed of several components is greater, but not much greater, than the sum of the components treated separately. Hence, the total torsional constant of the entire stiffener is approximated by the sum of the component torsional constants (27) and (28)

$$J_s > J_f + J_w = 0.0231\frac{A_f^{\,4}}{I_c} + \frac{1}{3}t_w^{\,3}\left(h_s - h_f\right) \tag{30}$$

In each finite element stiffener model, eleven distinct points establish the boundary of the bulb-flat stiffener cross-section (see Figure 7 and Appendix C). The boundary points define straight lines and 3-point arc curves. The curves define a single trimmed surface. The beam library provides the cross-sectional properties for the finite element models using the arbitrary shape option with the maximum allowable curvature error set at 0.005. Table 5 compares the area and torsional constant calculations with

finite element model results. Also, Table 5 compares the area and torsional constant calculations to published data from the Corus technical brochure [4].

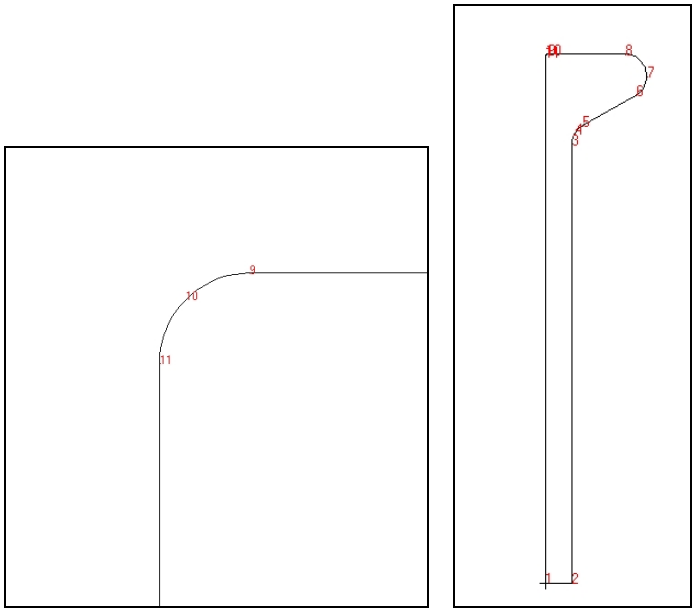

Figure 7 MSC Patran graphs of bulb-flat stiffener boundary points for cross-section properties

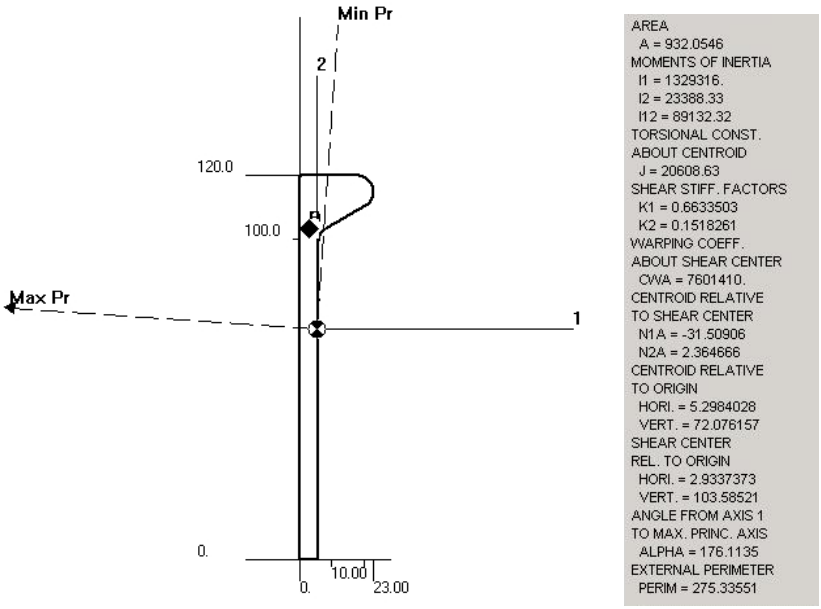

Figure 8 MSC Patran graph and data of a bulb-flat stiffener model

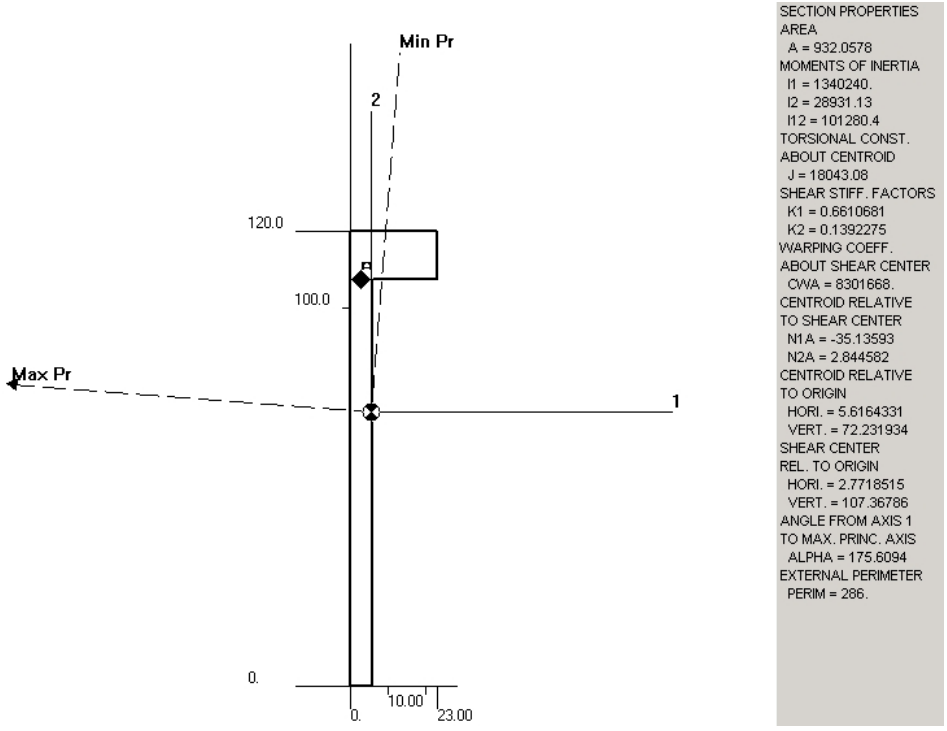

Figure 9 MSC Patran graph and data of an area-equivalent angle stiffener model

Table 5 Comparison of stiffener values

Variables h_s, t_w, t_{bf}, and r are given. $r_1 = (1/10)t_w$ and $\alpha = \pi/6$ radians.

Percent change = $\frac{J - J^{(FE)}}{J^{(FE)}} \times 100$. * - absolute percent change of less than 0.01%.

Source	t_w	t_{bf}	r	h_s	A_s	$I_{c-\text{stifffener}}$	Percent change	$J_{\text{stiffener}}$	Percent change
	mm	mm	mm	mm	mm^2	mm^4		mm^4	
Formula	6.0	17.0	5.0	120.0	932.06	1352719	*	20534	-0.37%
FE(bulb)					932.05	1352704	*	20609	*
FE(angle)					932.06	1369171	1.27%	18043	-12.45%
Corus					931.00	1353400	0.05%	15950	-22.61%
Formula	8.0	17.0	5.0	120.0	1172.00	1676051	*	33894	-0.91%
FE(bulb)					1172.00	1676034	*	34204	*
FE(angle)					1172.00	1694072	1.08%	30413	-11.08%
Corus					1170.00	1681000	0.30%	27730	-18.93%
Formula	7.0	19.0	5.5	140.0	1242.45	2448920	*	34535	-0.46%
FE(bulb)					1242.44	2448895	*	34694	*
FE(angle)					1242.44	2475783	1.10%	30482	-12.14%
Corus					1240.00	2448000	-0.04%	27080	-21.95%
Formula	10.0	19.0	5.5	140.0	1662.34	3206519	*	67721	-1.25%
FE(bulb)					1662.33	3206493	*	68575	*
FE(angle)					1662.34	3236434	0.93%	61791	-9.89%
Corus					1660.00	3215600	0.28%	57520	-16.12%
Formula	7.0	22.0	6.0	160.0	1460.10	3788414	*	47037	-0.26%
FE(bulb)					1460.09	3788380	*	47160	*
FE(angle)					1460.10	3831830	1.15%	41325	-12.37%
Corus					1460.00	3788600	*	36810	-21.95%
Formula	9.0	22.0	6.0	160.0	1780.03	4558106	*	70991	-0.65%
FE(bulb)					1780.02	4558068	*	71453	*
FE(angle)					1780.03	4605079	1.03%	63240	-11.49%
Corus					1780.00	4553200	-0.11%	57630	-19.35%
Formula	8.0	25.0	7.0	180.0	1885.81	6188305	*	70468	-0.26%
FE(bulb)					1885.80	6188242	*	80674	*
FE(angle)					1885.81	6261495	1.18%	70710	-12.35%
Corus					1890.00	6189000	0.01%	63520	-21.26%
Formula	10.0	25.0	7.0	180.0	2245.73	7289798	*	115017	-0.57%
FE(bulb)					2245.72	7289731	*	115672	*
FE(angle)					2245.73	7368371	1.08%	102123	-11.71%
Corus					2250.00	7290500	0.01%	93280	-19.36%

In Table 5, each stiffener model contains four rows of results. The four rows are referred to as a result set for clarity. Each row is data from a different source. The first row in each result set is data from the formulas for the bulb-flat cross-section. The second row in each set is data from the finite element analysis for the bulb-flat cross-section. The third row in each set is data from the finite element analysis for the area-equivalent angle cross-section. And the fourth row in each set is data from the Corus technical data brochure.

Comparing the first two rows of each stiffener result set compares the formula results to the finite element results. The independent sources agree almost exactly on the stiffener area values A_s and the values for the polar moments $I_{c-\text{stiffener}}$. The formula values for the torsional constants $J_{\text{stiffener}}$ obtained using the approximate expression (30) differs from the finite element values by less than two percent.

Comparing the second and third rows of each stiffener result set compares the finite element results of the bulb-flat to the finite element results of the area-equivalent angle cross-section. The two sources agree on the stiffener area values and the values for the polar moments. However there is a marked difference for the torsional constant values. Comparing the second and fourth rows of each stiffener result set compares the finite element results of the bulb-flat to the Corus technical data. The sources agree on the stiffener area values A_s and the values for the polar moments. The torsional constant values differ between 16% and 23%. The reason for the difference appears to be the lack of accuracy when using the idealization method to determine the torsional constant value.

In summary, this chapter presents expressions used to determine the planar properties of the bulb-flat cross-section. Stiffened plate analysis requires property value accuracy. Five independent parameters, web thickness, bulb thickness, two radii of curvature, and the slope angle uniquely define the bulb-flat flange geometry. The essential planar property formula (5) takes the form of an integral. All of the property values involve integral (5). The conventional methods of determining the torsional constant are not viable due to the asymmetrical cross-section of the bulb-flat geometry and the complicated equations that define the cross-section boundary. Expression (28) is developed from Saint Venant's one-term approximate expression and serves as a working

formula that yields very accurate results compared to finite element methods, thus supporting its validation. Using the approximate expression provides values that are more accurate than those obtained by idealizing the bulb-flat flange as an equivalent angle flange. The torsional constant for the bulb-flat stiffener is 15% - 23% higher than understood previously. In previous studies, the torsional nature of the bulb-flat was calculated using the torsional properties of an area-equivalent angle flange stiffener. From Table 5, the torque-carrying capacity of the bulb-flat stiffener is found to be greater than that of an area-equivalent angle stiffener.

III. STIFFENED PLATE BUCKLING

A. INTRODUCTION

This chapter deals with the buckling behavior of a stiffened plate. One method of analyzing the behavior of structural members is by deriving the governing differential equation and determining the exact solution using an appropriate differential equation technique. When the solution is difficult or impossible to determine, as is the case with stiffened plate structures, approximate methods of analysis are used. The Rayleigh-Ritz method is an effective alternate method that yields an approximate solution. The chapter presents an analytic expression for the buckling load of a rectangular stiffened plate, with one bulb-flat stiffener attached to one side, where the plate structure is subjected to axial compression. The results of the single stiffener analysis can be extended and applied to plate structures with more than one bulb-flat stiffener. Additionally, the analytic expression can be used to study the behavior of stiffened plates with different flange geometries.

B. ASSUMPTIONS

The fundamental assumptions are taken from Danielson [9], modified as appropriate, and stated as follows:

(i) Each plate-stiffener unit of width b undergoes an identical deformation.

(ii) The plate and web obey the nonlinear Von Karman plate equations (see Timoshenko and Gere [21]). The flange obeys the nonlinear beam equations derived by Bleich [1].

(iii) The plate and stiffener material is elastic, homogeneous, and isotropic.

(iv) Every particle on the bottom surface of a web undergoes the same displacement as the corresponding particle on the top surface of the plate, and every line of particles in a web normal to the plate surface remains normal to the deformed plate at its surface. In other words, the bases of the stiffeners are clamped to the plate.

(v) The prebuckling displacements are less than the maximum thickness of the structure and independent of the transverse coordinate.

(vi) The incremental buckling extensional strains at the midsurface of the plate and web are negligible.

(vii) The incremental buckling displacements may be approximated by the fundamental harmonic in their Fourier expansions.

(viii) The plate and web are so thin that their thicknesses are negligible compared to their width, length, and wavelength of deformation.

(ix) The stiffener flange has a solid cross-section with a length that is much greater than its largest cross-sectional dimension. Hence, the stiffener flange can be treated as a beam.

(x) The flange undergoes only lateral bending and torsion, no vertical bending.

C. ENERGY PRINCIPLE

The energy method for the solution of elastic stability problems is based on an extremum principle of mechanics that uses an energy criterion to characterize the equilibrium condition of the elastic system. A more precise statement of the energy criterion is made in Danielson [5] and is recapitulated in the following discussion.

Let P_I denote the potential energy of a system in equilibrium state I. Let P_{II} denote the potential energy in a neighborhood of equilibrium state I. Let $P[u]$ represent the increment in potential energy of the elastic system in transition by displacement field u from state I to a neighboring state. In addition, let $P[u]$ be expandable into the following component terms (functionals)

$$P[u] = P_1[u] + P_2[u] + P_3[u] + \cdots$$

where $P_1[u]$ refers to linear terms (functionals) with respect to u, $P_2[u]$ refers to quadratic terms (functionals) with respect to u, and so forth. Hence

$$P_{II} - P_I = P[u] = P_1[u] + P_2[u] + P_3[u] + \cdots$$

If $P[u] > 0$ for all non-vanishing neighborhoods of displacement fields u, then the fundamental equilibrium state I is stable. In a practical sense, stability here means that a force, stress, shock, or disturbance of the system does not cause an excessive change or dramatic departure of the equilibrium state to a neighboring state or configuration. If there exists a displacement field for which $P[u] < 0$, the fundamental equilibrium state I is unstable. Because the elastic system is in equilibrium, the linear term of the potential energy increment must vanish. That is, equilibrium requires $P_1[u] = 0$. The condition necessary for stability is $P_2[u] > 0$. The critical case of neutral equilibrium occurs when there exists a displacement field u_1 such that $P_2[u_1] = 0$ and $P_2[u \neq u_1] > 0$. In this case, the displacement field u_1 is the buckling mode, and the value of the load that corresponds to this displacement field is called the bifurcation-buckling load. Stated mathematically,

$$0 \leq P_2[u] \tag{31}$$

is the criterion used to determine the buckling mode and load given the properly defined total potential energy functional for the stiffened plate structure.

D. SIMPLY SUPPORTED RECTANGULAR STIFFENED PLATE

For the stiffened plate structure, the Cartesian coordinate system (x_1, x_2, x_3) is adopted from Danielson's work to aid result comparison and to minimize confusion with the flange cross-sectional coordinate systems (x, y) and (x_c, y_c). Consider a simply supported rectangular plate of length a, width b, and thickness t_p, with a longitudinal stiffener whose ends are also simply supported. The stiffener divides the width of the plate in halves and is composed of a thin web (treated as a plate element) of height h_w and thickness t_w, and a bulb-flat flange (treated as a beam-column element). Suppose the stiffened plate structure is under axial compression due to a uniform normal stress σ. The quadratic terms of the total potential energy functional for this single stiffened plate unit at the instance of buckling can be expressed as

$$P_2[W,V] = U_{\text{plate}} + U_{\text{web}} + U_{\text{flange}} - T_{\text{plate}} - T_{\text{web}} - T_{\text{flange}} \tag{32}$$

$W = W(x_1, x_2)$ and $V = V(x_1, x_3)$ are the deflection fields (modes) of the plate and stiffener, respectively. Subscripts on W and V denote partial differentiation with respect to the coordinate system, e.g. $W_{12} = \dfrac{\partial^2 W}{\partial x_1 \partial x_2}$. In expression (32), U_i denotes the internal potential energy as a result of strains for element i, and T_i denotes the potential energy of the external loads applied to element i. According to Timoshenko and Gere [21, pp. 337, 340, and 350] the internal potential energy expressions due to strains for the plate and web are taken as

$$U_{\text{plate}} = \frac{1}{2} D_p \int_{-\frac{b}{2}}^{\frac{b}{2}} \int_0^a \left\{ \left(W_{11} + W_{22}\right)^2 - 2(1-\nu)\left[W_{11}W_{22} - {W_{12}}^2 \right] \right\} dx_1 dx_2 \tag{33}$$

$$U_{\text{web}} = \frac{1}{2} D_w \int_0^{h_w} \int_0^a \left\{ \left(V_{11} + V_{33}\right)^2 - 2(1-\nu)\left[V_{11}V_{33} - {V_{13}}^2 \right] \right\} dx_1 dx_3 \tag{34}$$

The potential energy expression for the external loads applied to the plate and web are taken as

$$T_{\text{plate}} = \frac{1}{2} \sigma t_p \int_{-\frac{b}{2}}^{\frac{b}{2}} \int_0^a W_1^2 \, dx_1 dx_2 \tag{35}$$

$$T_{\text{web}} = \frac{1}{2} \sigma t_w \int_0^{h_w} \int_0^a V_1^2 \, dx_1 dx_3 \tag{36}$$

Due to assumption (x), the internal potential energy expression for the flange is

$$U_{\text{flange}} = \frac{1}{2} \int_0^a \left(EI_{xc} {V_{11}}^2 + GJ_f {V_{13}}^2 \right)_{x_3 = h_w} dx_1 \tag{37}$$

taken from Timoshenko and Gere [21, p. 25, eq. 1-52 and p. 265, eq. 6-30]. The value of I_{xc} is determined from expression (88).

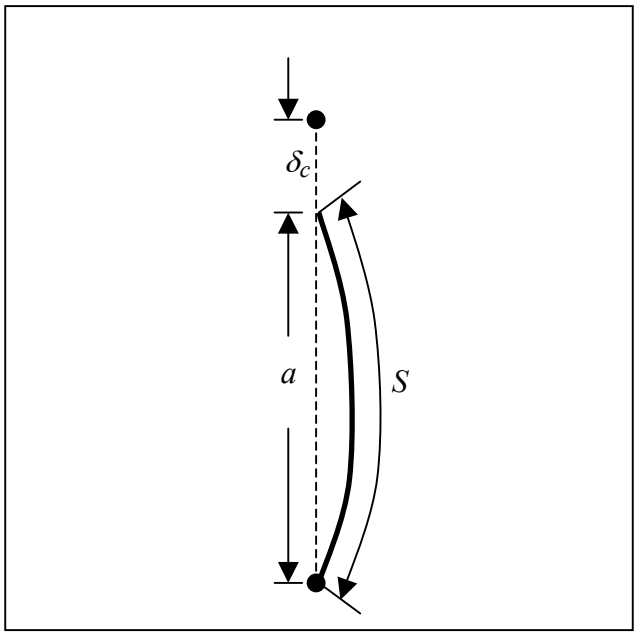

Figure 10 Top view of fiber curvature during buckling

The potential energy of the external load for the flange is the sum of the products of the external forces and the displacements of their points of application in the direction of the forces. As the flange buckles, the stresses on the end surfaces may change to $\sigma + d\sigma$. Considering small deformations, the assumption is that the end conditions are such that the work done by $d\sigma$ may be neglected in comparison with the work done by σ. Hence the change in potential energy for each fiber in the cross-section of the flange is

$$dT_{\text{flange}} = (\sigma dA)\delta_c \tag{38}$$

Each fiber carries a load σdA and displaces longitudinally a relative distance δ_c. The displacement is due to two reasons: the curvature of the fiber and the change in the longitudinal stress. Bleich explains and shows that the potential energy due to the change in longitudinal stress vanishes. Hence the change in potential energy for each fiber is due to fiber curvature only. The potential energy of the external load for the flange is derived here and follows the outline in Bleich [1, pp. 126-127] and Chajes [2, pp. 204-207].

Let δ_c denote the relative fiber displacement due to the curvature of the flange as it buckles under axial compression. The distance δ_c is equal to the difference between the arc length S of the fiber due to bending and the chord length a of the fiber. Hence

$$\delta_c = S - a$$

The potential energy of the external load for the flange is obtained by integrating over the cross-sectional area of the flange. Thus

$$T_{\text{flange}} = \sigma \iint_A \delta_c dx_2 dx_3 \tag{39}$$

To determine δ_c, consider a cross-section of the flange at distance x_1 along the length of the flange. The centroid of the cross-section coincides with the coordinate origin.

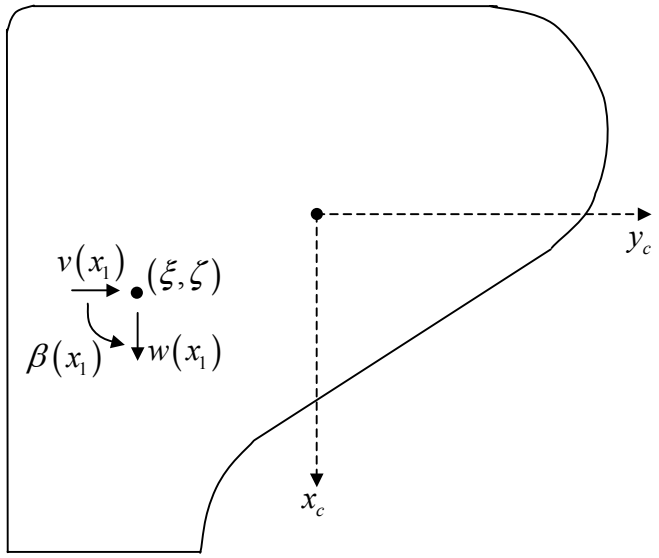

Figure 11 Flange cross-section with centroidal coordinate system

Due to buckling, the point with coordinates (x_c, y_c) in the cross-section of the flange will change coordinates to $(x_c + \Delta x_c, y_c + \Delta y_c)$, where Δx_c and Δy_c are functions of x_1. Let the point of rotation of the cross-section have coordinates (ξ, ζ) relative to the centroid of the cross-section. Movements of the point of rotation define the displacement of

points in the cross-section: $w(x_1)$ in the x_c direction, $v(x_1)$ in the y_c direction, and $\beta(x_1)$ counterclockwise rotation about the point of rotation. Hence

$$\begin{bmatrix}\Delta x_c\\ \Delta y_c\end{bmatrix}=\begin{bmatrix}\cos\beta & -\sin\beta\\ \sin\beta & \cos\beta\end{bmatrix}\begin{bmatrix}x_c-\xi+w\\ y_c-\zeta+v\end{bmatrix}-\begin{bmatrix}x_c-\xi\\ y_c-\zeta\end{bmatrix}$$

Since only small deformations are considered, simplification of the right-hand side gives

$$\begin{bmatrix}\Delta x_c\\ \Delta y_c\end{bmatrix}=\begin{bmatrix}1 & -\beta\\ \beta & 1\end{bmatrix}\begin{bmatrix}x_c-\xi+w\\ y_c-\zeta+v\end{bmatrix}-\begin{bmatrix}x_c-\xi\\ y_c-\zeta\end{bmatrix}=\begin{bmatrix}w-(y_c-\zeta)\beta-v\beta\\ v+(x_c-\xi)\beta+w\beta\end{bmatrix}$$

Using the Pythagorean theorem, and considering $\frac{d\Delta x_c}{dx_1}=\Delta x_c'$ and $\frac{d\Delta y_c}{dx_1}=\Delta y_c'$ to be small, yields

$$\delta_c=S-a=\int_0^a\left\{\left[1+\left(\Delta x_c'\right)^2+\left(\Delta y_c'\right)^2\right]^{1/2}-1\right\}dx_1\approx\frac{1}{2}\int_0^a\left[\left(\Delta x_c'\right)^2+\left(\Delta y_c'\right)^2\right]dx_1$$

The potential energy of the external load for the flange is given by

$$T_{\text{flange}}=\frac{1}{2}\sigma\iint_A\int_0^a\left[\left(\Delta x_c'\right)^2+\left(\Delta y_c'\right)^2\right]dx_1dx_cdy_c \tag{40}$$

Using the geometrical relations for the area, first and second moments of the flange cross-section (assuming the centroid and coordinate origin coincide),

$$\iint_R dx_cdy_c=A_f$$
$$\iint_R x_cdx_cdy_c=\iint_R y_cdx_cdy_c=0$$
$$\iint_R(x_c-\xi)^2+(y_c-\zeta)^2\,dx_cdy_c=I_f$$

the quadratic terms of the potential energy due to external loads are given by

$$T_{\text{flange}}=\frac{1}{2}\sigma\int_0^a\left[A_f\left(v'^2+w'^2\right)-2A_f\xi v'\beta'+2A_f\zeta w'\beta'+I_f\beta'^2\right]dx_1 \tag{41}$$

Movements in the x_c direction affected by $w(x_1)$ are assumed negligible, by assumption (x), compared to y_c direction movements perpendicular to the surface of the web yielding

$$T_{\text{flange}} = \frac{1}{2}\sigma\int_0^a \left(A_f v'^2 - 2A_f \xi v'\beta' + I_f \beta'^2 \right) dx_1 \tag{42}$$

The point of rotation of the cross-section is taken to be the point centered on and at the top of the web. This selection provides continuity of the motion at the top of the web and the flange. The point of rotation is located half way between points 4 and 5 as shown in Figure 3 found on page 9. Relative to the orientation of the flange, ξ is the vertical distance from the centroid to the point of rotation. For the bulb-flat cross-section

$$\xi = h_f - \overline{x} = -\left(\overline{x} - h_f\right) \tag{43}$$

and

$$I_f = I_c + A_f\left[\left(\overline{x} - h_f\right)^2 + \left(\overline{y} - \frac{1}{2}t_w\right)^2\right] \tag{44}$$

where $\overline{x}$ is determined from (83) and $\overline{y}$ is determined from (84). A lateral movement of the point of rotation $v(x_1)$ equates to $V(x_1, h_w)$. A rotation or twist about the point of rotation of the flange $\beta(x_1)$ equates to $V_3(x_1, h_w)$.

1. Energy Functional

The quadratic terms of the total potential energy functional of a single stiffened plate unit at the instance of buckling can be expressed as

$$\begin{aligned} P_2 &= U_{plate} + U_{web} + U_{flange} - T_{plate} - T_{web} - T_{flange} \\ &= \frac{1}{2} D_p \int_{-\frac{b}{2}}^{\frac{b}{2}} \int_0^a \left\{ \left(W_{11} + W_{22} \right)^2 - 2\left(1-\nu\right)\left[W_{11} W_{22} - {W_{12}}^2 \right] \right\} dx_1 dx_2 \\ &+ \frac{1}{2} D_w \int_0^{h_w} \int_0^a \left\{ \left(V_{11} + V_{33} \right)^2 - 2\left(1-\nu\right)\left[V_{11} V_{33} - {V_{13}}^2 \right] \right\} dx_1 dx_3 + \frac{1}{2} \int_0^a \left(EI_{xc} {V_{11}}^2 + GJ_f {V_{13}}^2 \right)_{x_3 = h_w} dx_1 \\ &- \frac{1}{2} \sigma \left[\int_{-\frac{b}{2}}^{\frac{b}{2}} \int_0^a t_p W_1^2 dx_1 dx_2 + \int_0^{h_w} \int_0^a t_w V_1^2 dx_1 dx_3 + \int_0^a \left(A_f V_1^2 + 2A_f \left(\overline{x} - h_f \right) V_1 V_{13} + I_f {V_{13}}^2 \right)_{x_3 = h_w} dx_1 \right] \end{aligned} \tag{45}$$

The boundary conditions of the stiffened plate structure are

$$W\left(0, x_2\right) = W\left(a, x_2\right) = 0 \tag{46}$$

$$W_{11}\left(0, x_2\right) = W_{11}\left(a, x_2\right) = 0 \tag{47}$$

$$V\left(0, x_3\right) = V\left(a, x_3\right) = 0 \tag{48}$$

$$V_{11}\left(0, x_3\right) = V_{11}\left(a, x_3\right) = 0 \tag{49}$$

$$V\left(x_1, 0\right) = W\left(x_1, 0\right) \tag{50}$$

$$V_3\left(x_1, 0\right) = W_2\left(x_1, 0\right) \tag{51}$$

2. Approximate Solution

The Rayleigh-Ritz method is a very effective technique that finds an approximate solution to problems requiring the first variation of the total potential energy functional to vanish. The method is summarized in two steps. First, assume an admissible solution containing unknown coefficients that satisfy the boundary conditions of the problem. Second, substitute the assumed solution into the functional and determine the value of the unknown coefficients that minimizes the functional. From experimental observation and by assumption (vii), the deflection of the plate panel is assumed

$$W\left(x_1, x_2\right) = c \sin \frac{m\pi x_1}{a} \sin \frac{\pi x_2}{b} \tag{52}$$

where c is an arbitrary constant. The value m is the number of half waves in the buckling mode along the longitudinal axis and is taken to be the integer that gives the lowest value for the buckling load. The deflection of the stiffener is assumed

$$V\left(x_1, x_3\right) = c \sin \frac{m\pi x_1}{a} f\left(x_3\right) \tag{53}$$

where $f\left(x_3\right)$ is a function to be determined. Expressions (52) and (53) satisfy boundary conditions (46) - (49). Boundary conditions (50) and (51) transform to the following conditions:

$$f\left(0\right) = 0 \tag{54}$$

$$f'\left(0\right) = \frac{\pi}{b} \tag{55}$$

Hence,

$$P_2 = \frac{1}{4} \frac{c^2 m^2 \pi^4}{ab^2} \left\langle \frac{1}{2} D_p b \left(\frac{mb}{a} + \frac{a}{mb} \right)^2 + \text{Term}_1 + EI_{xc} \frac{m^2 b^2}{a^2} f\left(h_w\right)^2 + GJ_f \frac{b^2}{\pi^2} f'\left(h_w\right)^2 - \sigma \text{Term}_2 \right\rangle$$

$$\text{Term}_1 = D_w \frac{b^2}{\pi^2} \int \left\{ \left[\frac{m\pi}{a} f\left(x_3\right) - \frac{a}{m\pi} f''\left(x_3\right) \right]^2 + 2\left(1-\nu\right) \left[f\left(x_3\right) f''\left(x_3\right) + f'\left(x_3\right)^2 \right] \right\} dx_3$$

$$\text{Term}_2 = \frac{t_p b^3}{2\pi^2} + t_w \frac{b^2}{\pi^2} \int f\left(x_3\right)^2 dx_3 + A_f \frac{b^2}{\pi^2} f\left(h_w\right)^2 + 2A_f \left(\overline{x} - h_f\right) \frac{b^2}{\pi^2} f\left(h_w\right) f'\left(h_w\right) + I_f \frac{b^2}{\pi^2} f'\left(h_w\right)^2 \tag{56}$$

where the omitted limits of integration are from $x_3 = 0$ to $x_3 = h_w$.

Applying the stability criteria (31) yields

$$\sigma_{cr} \le \frac{\frac{1}{2}D_p b\left(\frac{mb}{a}+\frac{a}{mb}\right)^2 + \text{Term}_1 + EI_{xc}\frac{m^2b^2}{a^2}f\left(h_w\right)^2 + GJ_f\frac{b^2}{\pi^2}f'\left(h_w\right)^2}{\frac{t_p b^3}{2\pi^2} + t_w\frac{b^2}{\pi^2}\int f\left(x_3\right)^2 dx_3 + A_f\frac{b^2}{\pi^2}f\left(h_w\right)^2 + 2A_f\left(\overline{x}-h_f\right)\frac{b^2}{\pi^2}f\left(h_w\right)f'\left(h_w\right) + I_f\frac{b^2}{\pi^2}f'\left(h_w\right)^2}$$

$$\text{Term}_1 = D_w\frac{b^2}{\pi^2}\int\left\{\left[\frac{m\pi}{a}f\left(x_3\right)-\frac{a}{m\pi}f''\left(x_3\right)\right]^2 + 2\left(1-\nu\right)\left[f\left(x_3\right)f''\left(x_3\right)+f'\left(x_3\right)^2\right]\right\}dx_3 \tag{57}$$

where a proper selection of $f\left(x_3\right)$ minimizes the upper bound for the buckling load.

Notice that in the case of a plate panel with no stiffener, only the first terms of the numerator and denominator in (57) remain and the buckling load value is

$$\sigma_{cr} \le \frac{\frac{1}{2}D_p b\left(\frac{mb}{a}+\frac{a}{mb}\right)^2}{\frac{t_p b^3}{2\pi^2}} = D_p\frac{\pi^2}{t_p b^2}\left(\frac{mb}{a}+\frac{a}{mb}\right)^2 \tag{58}$$

where m is one of the two integers closest to a/b. Expression (58) agrees with the well-known solution for the buckling of a plate that has length a, width b, and is simply supported at all edges.

When there is a thin-webbed stiffener but no flange, the web deflection assumes the form

$$f\left(x_3\right) = \frac{\pi x_3}{b} \tag{59}$$

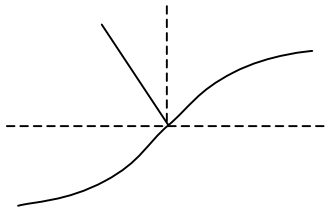

Figure 12 Plate and web deflection when there is no flange

and the buckling load is the value

$$\sigma_{cr} \le \frac{\frac{1}{2} D_p b \left(\frac{mb}{a} + \frac{a}{mb} \right)^2 + D_w h_w \left[\frac{1}{3} \left(\frac{m\pi h_w}{a} \right)^2 + 2(1-\nu) \right]}{\frac{t_p b^3}{2\pi^2} + \frac{t_w h_w{}^3}{3}} \tag{60}$$

3. General Buckling Mode and Load

Common conjectures for $f(x_3)$ include

$$f_1(x_3) = \frac{h_w}{b} \sin \frac{\pi x_3}{h_w} \tag{61}$$

$$f_2(x_3) = \sin \frac{\pi x_3}{b} \tag{62}$$

$$f_3(x_3) = \frac{\pi x_3}{b} \tag{63}$$

Expressions (61) - (63) satisfy boundary conditions (54) and (55).

$$f_1(0) = f_2(0) = f_3(0) = 0$$

$$f_1'(0) = f_2'(0) = f_3'(0) = \frac{\pi}{b}$$

When (61) - (63) are substituted into (53), they yield the following stiffener deflection approximations:

$$V_1(x_1, x_3) = c \sin\frac{m\pi x_1}{a}\left(\frac{h_w}{b}\sin\frac{\pi x_3}{h_w}\right)$$

$$V_2(x_1, x_3) = c \sin\frac{m\pi x_1}{a}\left(\sin\frac{\pi x_3}{b}\right)$$

$$V_3(x_1, x_3) = c \sin\frac{m\pi x_1}{a}\left(\frac{\pi x_3}{b}\right)$$

Linear combinations of (61) - (63) are often used to achieve better accuracy in approximating the stiffener deflection. The deflection mode function can be assumed in the form of a series of functions with undetermined coefficients. If the series of functions is complete, by increasing the number of terms in the series the approximation for the buckling load converges from above to the exact buckling load value. Functions (61) - (63) belong to a family of functions whose members satisfy the boundary conditions. Functions belonging to such a family are of the form

$$f(x_3) = \frac{\mu h_w}{b}\sin\frac{\pi x_3}{\mu h_w}, \quad \mu \neq 0 \tag{64}$$

Note that

$$\lim_{|\mu|\to\infty} f(x_3) = \lim_{|\mu|\to\infty}\left(\frac{\mu h_w}{b}\sin\frac{\pi x_3}{\mu h_w}\right) = \frac{\pi x_3}{b}$$

Continuing with the Rayleigh-Ritz method, substitution of the assumed web deflection (64) into the general buckling load expression (57) yields

$$\sigma_{cr} \le \frac{\frac{1}{2}D_p b\left(\frac{mb}{a}+\frac{a}{mb}\right)^2 + \text{Term}_1 + EI_{xc}\left(\frac{m\pi h_w}{a}\right)^2\left(\frac{\mu}{\pi}\sin\frac{\pi}{\mu}\right)^2 + GJ_f\left(\cos\frac{\pi}{\mu}\right)^2}{\frac{t_p b^3}{2\pi^2}+\frac{t_w h_w{}^3\mu^2}{2\pi^2}\left(1-\frac{\mu}{2\pi}\sin\frac{2\pi}{\mu}\right)+\text{Term}_2}$$

$$\text{Term}_1 = \frac{1}{2}D_w h_w\left[\left(\frac{m\mu h_w}{a}+\frac{a}{m\mu h_w}\right)^2\left(1-\frac{\mu}{2\pi}\sin\frac{2\pi}{\mu}\right)+4(1-\nu)\frac{\mu}{2\pi}\sin\frac{2\pi}{\mu}\right] \tag{65}$$

$$\text{Term}_2 = A_f h_w{}^2\left(\frac{\mu}{\pi}\sin\frac{\pi}{\mu}\right)^2 + 2A_f(\bar{x}-h_f)h_w\left(\frac{\mu}{\pi}\sin\frac{\pi}{\mu}\right)\left(\cos\frac{\pi}{\mu}\right)+I_f\left(\cos\frac{\pi}{\mu}\right)^2$$

where the value of μ is chosen to minimize the expression. One method of determining μ is by setting equal to zero the ordinary derivative of the quotient expression (65) with respect to μ and solving for μ. The value can also be obtained graphically. Three special values $\mu = 1$, $\mu = 2$, and $\mu \to \infty$ relate to three special deflection modes.

For $\mu = 1$, the deflection mode becomes $f(x_3) = \frac{h_w}{b} \sin \frac{\pi x_3}{h_w}$ and the buckling load is

$$\sigma_{cr} \le \frac{\frac{1}{2} D_p b \left(\frac{mb}{a} + \frac{a}{mb} \right)^2 + \frac{1}{2} D_w h_w \left(\frac{mh_w}{a} + \frac{a}{mh_w} \right)^2 + GJ_f}{\frac{t_p b^3}{2\pi^2} + \frac{t_w h_w^3}{2\pi^2} + I_f} \tag{66}$$

Figure 13 depicts the deflection of the structure corresponding to mode 1 that is best described by a bending of the web in one half-wave and a rotation of the flange about a point at the top of the web. There is no flange bending along its length. Such a mode could occur when the flange bending stiffness is large compared to flange torsion and web bending. An example of this occurrence is a wide T flange combined with a thin web possessing relatively low flexural rigidity.

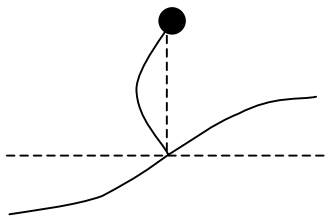

Figure 13 Mode 1 deflection

For $\mu = 2$, the deflection mode becomes $f(x_3) = \frac{2h_w}{b}\sin\frac{\pi x_3}{2h_w}$ and the buckling load is

$$\sigma_{cr} \le \frac{\frac{1}{2}D_p b\left(\frac{mb}{a}+\frac{a}{mb}\right)^2 + \frac{1}{2}D_w h_w\left(\frac{2mh_w}{a}+\frac{a}{2mh_w}\right)^2 + 4EI_{xc}\left(\frac{mh_w}{a}\right)^2}{\frac{t_p b^3}{2\pi^2}+\frac{2t_w h_w^{\,3}}{\pi^2}+4A_f\left(\frac{h_w}{\pi}\right)^2} \tag{67}$$

Figure 14 depicts the deflection of the structure corresponding to mode 2. This deflection corresponds to a significant bending of the flange and web with no flange torsion. This mode could occur when the flange torsional stiffness is large compared to flange and web bending.

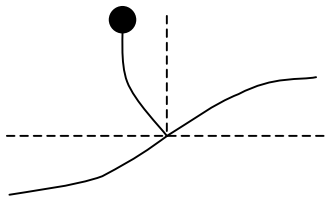

Figure 14 Mode 2 deflection

For $\mu \to \infty$, the deflection mode becomes $f(x_3) = \frac{\pi x_3}{b}$ and the buckling load is

$$\sigma_{cr} \le \frac{\frac{1}{2}D_p b\left(\frac{mb}{a}+\frac{a}{mb}\right)^2 + D_w h_w\left[\frac{1}{3}\left(\frac{m\pi h_w}{a}\right)^2 + 2(1-\nu)\right] + EI_{xc}\left(\frac{m\pi h_w}{a}\right)^2 + GJ_f}{\frac{t_p b^3}{2\pi^2}+\frac{t_w h_w^{\,3}}{3}+A_f h_w^{\,2}+2A_f\left(\bar{x}-h_f\right)h_w + I_f} \tag{68}$$

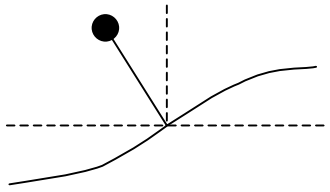

Figure 15 Mode 3 deflection

Figure 15 depicts the deflection of the structure corresponding to mode 3. This deflection corresponds to the flange exhibiting a combination of bending and twisting while the web tends to remain straight. Such a mode could occur when the web flexural stiffness is

large compared to flange bending and torsion effects. This case is likely to occur when the flange offers little or no additional stiffness to the plate structure compared to the contribution of the web.

The value of μ can be interpreted to indicate the deflection behavior based on the three special deflection modes.

Mode	μ	Flange bending	Flange torsion	Web bending
1	1	No	Yes	Yes
2	2	Yes	No	Yes
3	∞	Yes	Yes	No

4. Buckling Expression Summary

The following summarizes the analytic expressions that predict the critical buckling load and buckling behavior of a rectangular stiffened plate with a thin webbed stiffener and solid flange treated as a beam. The general expression involves a constant μ determined graphically. The value of μ indicates the deflection behavior.

General Buckling Load Expression $(\mu \neq 0)$

$$\sigma_{cr} \leq \frac{\frac{1}{2}D_p b\left(\frac{mb}{a}+\frac{a}{mb}\right)^2+\frac{1}{2}D_w h_w\left[\left(\frac{m\mu h_w}{a}+\frac{a}{m\mu h_w}\right)^2\left(1-\frac{\mu}{2\pi}\sin\frac{2\pi}{\mu}\right)+4(1-\nu)\frac{\mu}{2\pi}\sin\frac{2\pi}{\mu}\right]+EI_{xc}\left(\frac{m\pi h_w}{a}\right)^2\left(\frac{\mu}{\pi}\sin\frac{\pi}{\mu}\right)^2+GJ_f\left(\cos\frac{\pi}{\mu}\right)^2}{\frac{t_p b^3}{2\pi^2}+\frac{t_w h_w{}^3\mu^2}{2\pi^2}\left(1-\frac{\mu}{2\pi}\sin\frac{2\pi}{\mu}\right)+A_f h_w{}^2\left(\frac{\mu}{\pi}\sin\frac{\pi}{\mu}\right)^2+2A_f\left(\bar{x}-h_f\right)h_w\left(\frac{\mu}{\pi}\sin\frac{\pi}{\mu}\right)\left(\cos\frac{\pi}{\mu}\right)+I_f\left(\cos\frac{\pi}{\mu}\right)^2}$$

Mode 1 Expression $(\mu = 1)$

$$\sigma_{cr} \leq \frac{\frac{1}{2}D_p b\left(\frac{mb}{a}+\frac{a}{mb}\right)^2+\frac{1}{2}D_w h_w\left(\frac{mh_w}{a}+\frac{a}{mh_w}\right)^2+GJ_f}{\frac{t_p b^3}{2\pi^2}+\frac{t_w h_w{}^3}{2\pi^2}+I_f}$$

Mode 2 Expression $(\mu = 2)$

$$\sigma_{cr} \leq \frac{\frac{1}{2}D_p b\left(\frac{mb}{a}+\frac{a}{mb}\right)^2+\frac{1}{2}D_w h_w\left(\frac{2mh_w}{a}+\frac{a}{2mh_w}\right)^2+4EI_{xc}\left(\frac{mh_w}{a}\right)^2}{\frac{t_p b^3}{2\pi^2}+\frac{2t_w h_w{}^3}{\pi^2}+4A_f\left(\frac{h_w}{\pi}\right)^2}$$

Mode 3 Expression $(\mu \to \infty)$

$$\sigma_{cr} \leq \frac{\frac{1}{2}D_p b\left(\frac{mb}{a}+\frac{a}{mb}\right)^2+D_w h_w\left[\frac{1}{3}\left(\frac{m\pi h_w}{a}\right)^2+2(1-\nu)\right]+EI_{xc}\left(\frac{m\pi h_w}{a}\right)^2+GJ_f}{\frac{t_p b^3}{2\pi^2}+\frac{t_w h_w{}^3}{3}+A_f h_w{}^2+2A_f\left(\bar{x}-h_f\right)h_w+I_f}$$

The three special mode expressions provide initial approximations for the upper bound of the buckling load value. Once the proper value of μ is estimated, the general expression provides a value that is less than or equal to the lowest initial approximation.

5. Example

As an example, consider a stiffened plate structure, simply supported on all sides, subjected to an axial compression load along the longitudinal axis, with the following parameters.

Material properties:

$$E = 30,000 \text{ ksi} \quad \nu = 0.3$$

Plate properties:

$$a = 72 \text{ inches} = 1829 \text{ mm}$$
$$b = 20 \text{ inches} = 508 \text{ mm}$$
$$t_p = 0.3125 \text{ inches} = 7.9375 \text{ mm}$$

Web properties:

$$h_s = 4.1338 \text{ inches} = 105 \text{ mm}$$
$$t_w = 0.2362 \text{ inches} = 6 \text{ mm}$$

Bulb-flat flange properties:

$$t_{bf} = 0.6693 \text{ inches} = 17 \text{ mm}$$
$$r = 0.1969 \text{ inches} = 5 \text{ mm}$$
$$r_1 = 0.0236 \text{ inches} = 0.6 \text{ mm}$$
$$\alpha = \pi/6 \text{ radians} = 30^0$$

A Maple 8 worksheet provides:

$$D_p = 83840 \quad D_w = 36212 \quad m = 4 \quad h_w = 3.3233$$
$$h_f = 0.8106 \quad A_f = 0.5202 \quad \bar{x} = 0.3214 \quad \bar{y} = 0.3694$$
$$I_{xc} = 0.0309 \quad J_f = 0.0321 \quad I_f = 0.2100$$
$$EI_{xc} = 926071 \quad GJ_f = 370796$$

The following figure shows the graph of the general expression for the buckling load of the plate with a bulb-flat stiffener.

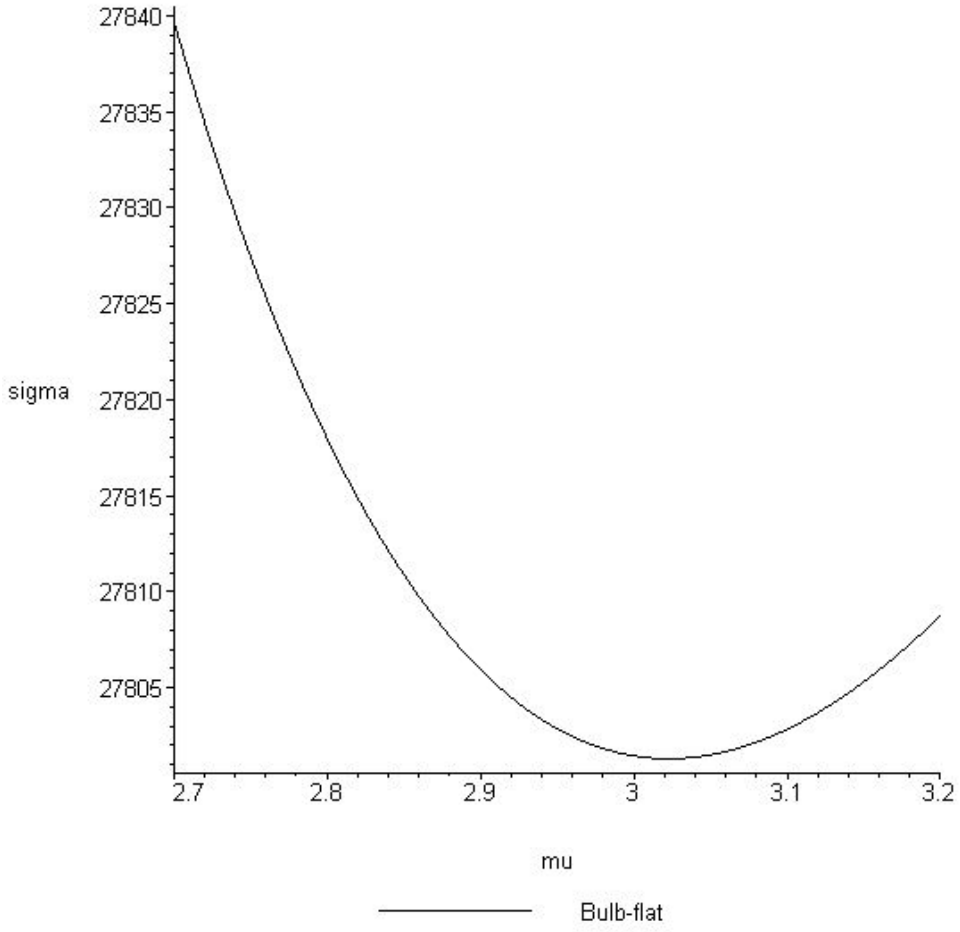

Figure 16 Maple 8 graph of the buckling load for the bulb-flat stiffened plate example

Table 6 Results for the bulb-flat stiffened plate example

Description	$\sigma \leq$ Buckling Load (psi)	Remarks
Plate without stiffener	26773	(58)
Plate stiffened with no flange	27581	(60) 3.02% above the no stiffener value.
Mode 1	44380	(66)
Mode 2	31262	(67)
Mode 3	31801	(68)
General Expression	27802	Graphically and (65). $\mu = 3.02$ 3.84% above the no stiffener value. 0.80% above the no flange value.

Without stiffening, the plate is predicted to buckle at a load less than or equal to 26773 psi. When a flangeless web of height $h_w = 3.3233$ in. is added to the plate panel, the plate buckles at a load of less than or equal to 27581 psi. Based on the value for μ, the buckling behavior is predicted to exhibit flange bending and torsion with relatively little web bending. The given flange cross-section adds relatively little additional stiffness compared to the web stiffness.

E. FINITE ELEMENT ANALYSIS

Numerical and experimental investigations give insight about the behavior of stiffened plates and serve as a basis of comparison to theoretical predictions. The results of finite element analyses for several stiffened plate models using MSC Nastran 2001/Patran 2001-r3 software are compared to analytical predictions to establish a degree of confirmation.

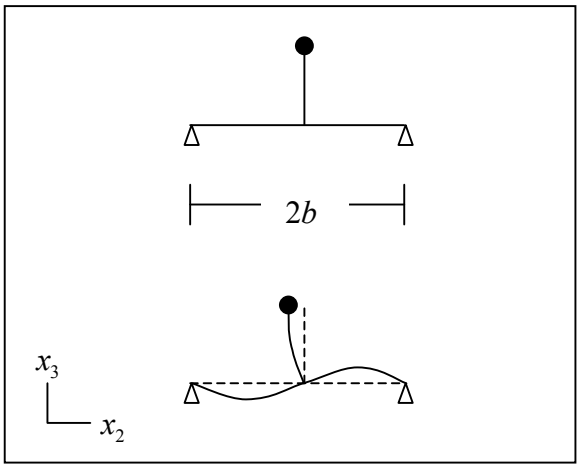

Figure 17 Stiffened plate pre-buckling and buckling mode

Several simply supported rectangular plate structures serve as finite element models. Each plate structure has a plate panel of length a, width $2b$, and thickness t_p such that $t_p \ll b < a$. The stiffener divides the width of the plate in halves. Each plate panel half extends b units of length from the web to the simply supported edge. The stiffener includes a thin web of length a, height h_w, and thickness t_w such that $t_w \ll h_w < a$. Four flange configurations are examined: no flange, bulb-flat flange, circular flange, and T-flange. Each stiffened plate structure is subjected to axial compression due to a uniform normal stress σ, which increases to the buckling load. The boundary of the plate panel is simply supported at all edges. The stiffener is simply supported at the ends.

The derived analytical expressions in the previous section were modeled assuming a plate panel of width b. This coincides with the analysis of a single plate unit containing a single longitudinal stiffener that would be part of a larger plate structure where b units of length separate each stiffener. In this discussion, the plate structure is modeled with width $2b$, as shown in Figure 17. The boundary conditions are now

$$W\left(x_1,-b\right)=W\left(x_1,b\right)=0$$
$$W_{22}\left(x_1,-b\right)=W_{22}\left(x_1,b\right)=0$$

Consistency with the finite element model analysis of the $2b$ width model requires changing the limits of integration associated with the plate energy terms U_{plate} and T_{plate} from $x_2 = \pm b/2$ to $x_2 = \pm b$. The fundamental problem and its mode shapes remain unchanged.

A secondary aim of the finite element analysis is to estimate the effects of several variables or factors. The intention is to discern the sensitivity of the analytic expression accuracy due to the variability of web height, flange area, and flange configuration. The web height variable is examined at two levels, the flange area at four levels, and the flange configuration at four levels. The plate panel parameters for all models remain fixed at the following values:

$$a = 72 \text{ inches } = 1829 \text{ mm}$$
$$b = 20 \text{ inches } = 508 \text{ mm}$$
$$t_p = 0.3125 \text{ inches } = 7.9375 \text{ mm}$$

A 105 mm stiffener with a bulb-flat flange (see model 1 from Table 2) has a web height of 84.41 mm. This is the web height used for the first set of plate models. A 120 mm stiffener with a bulb-flat flange (see model 1 from Table 2) has a web height of 99.41 mm. This is the web height used for the second set of plate models. The web thickness is fixed at 6 mm.

$$\text{Web height 1: } h_w = 84.41 \text{ mm}$$
$$\text{Web height 2: } h_w = 99.41 \text{ mm}$$
$$\text{Web thickness: } t_w = 6 \text{ mm}$$

There are four flange areas examined. The first case is that for a stiffener with no flange. The remaining flange area values are derived from the following bulb-flat flange parameters (units in mm) where $r_1 = (1/10)t_w$ and $\alpha = \pi/6$.

Flange Area Level	t_w	t_{bf}	r	Area (mm^2)
1	N/A	N/A	N/A	0
2	6	17	5	335.59
3	6	20	5	401.69
4	6	25	5	523.39

The flange parameters used for area levels 3 and 4 are not from the data in Table 2 or Table 3. Analyses of these bulb-flat flanges provide an assessment of the prediction accuracy for non-standard parameters. The four flange configurations examined are

Flange Configuration	Label	Description
1	N/A	No flange
2	b	Bulb-flat
3	c	Circular
4	t	T-flange

For the stiffened plate structure without a flange, the web deflection mode is of the form (59) and the predicted buckling load is determined by

$$\sigma_{cr} \le \frac{D_p b\left(\frac{mb}{a}+\frac{a}{mb}\right)^2 + D_w h_w\left[\frac{1}{3}\left(\frac{m\pi h_w}{a}\right)^2 + 2(1-\nu)\right]}{\frac{t_p b^3}{\pi^2}+\frac{t_w h_w{}^3}{3}}$$

Otherwise the stiffener has a flange and the web deflection is of the form (64) with the predicted buckling load determined by

$$\sigma_{cr} \le \frac{D_p b\left(\frac{mb}{a}+\frac{a}{mb}\right)^2 + \frac{1}{2}D_w h_w\left[\left(\frac{m\mu h_w}{a}+\frac{a}{m\mu h_w}\right)^2\left(1-\frac{\mu}{2\pi}\sin\frac{2\pi}{\mu}\right)+4(1-\nu)\frac{\mu}{2\pi}\sin\frac{2\pi}{\mu}\right] + EI_{xc}\left(\frac{m\pi h_w}{a}\right)^2\left(\frac{\mu}{\pi}\sin\frac{\pi}{\mu}\right)^2 + GJ_f\left(\cos\frac{\pi}{\mu}\right)^2}{\frac{t_p b^3}{\pi^2}+\frac{t_w h_w{}^3\mu^2}{2\pi^2}\left(1-\frac{\mu}{2\pi}\sin\frac{2\pi}{\mu}\right)+A_f h_w{}^2\left(\frac{\mu}{\pi}\sin\frac{\pi}{\mu}\right)^2+2A_f(\bar{x}-h_f)h_w\left(\frac{\mu}{\pi}\sin\frac{\pi}{\mu}\right)\left(\cos\frac{\pi}{\mu}\right)+I_f\left(\cos\frac{\pi}{\mu}\right)^2}$$

Using the values from the previous two pages and converting the units from millimeter to inches provides the parameters for the stiffened plate models. The following tables present the converted parameter values. The data tables in Appendix C for the stiffened plate finite element models are in inch units (See Table 40 - Table 55). Converting the results back into millimeter units may yield values that differ slightly from those presented in previous sections.

Table 7 Summary of stiffened plate model 1 parameters

Configuration	Flange Parameters and Properties	Web Parameters
Model 1	$A_f = 0.5202$ in^2	$h_w = 3.3233$ in $t_w = 0.2362$ in
No flange See Table 40	No flange area	Same as above
Bulb-flat (b) See Table 42[7]	$t_w = 0.2362$ in $t_{bf} = 0.6693$ in $r = 0.1969$ in $r_1 = (1/10)t_w = 0.0236$ in $\alpha = \pi/6$ radians $h_f = 0.8106$ in	$h_s = 4.1339$ in
Circular (c) See Table 48	radius = 0.4069 in $h_f = 0.8138$ in	$h_s = 4.1371$ in
T-flange (t) See Table 54	width = 2.2020 in thickness = 0.2362 in	$h_s = 3.5595$ in

[7] The parameters for this model configuration were used in a grillage tested by the Naval Surface Warfare Center. The flange and web parameters are the same as used in the example on page 52.

Table 8 Summary of stiffened plate model 2 parameters

Configuration	Flange Parameters	Web Parameters
Model 2	$A_f = 0.6226 \text{ in}^2$	$h_w = 3.3233$ in $t_w = 0.2362$ in
No flange See Table 40	No flange area	Same as above
Bulb-flat (b) See Table 43	$t_w = 0.2362$ in $t_{bf} = 0.7874$ in $r = 0.1969$ in $r_1 = (1/10)t_w = 0.0236$ in $\alpha = \pi/6$ radians $h_f = 0.8788$ in	$h_s = 4.2021$ in
Circular (c) See Table 49	radius = 0.4452 in $h_f = 0.8904$ in	$h_s = 4.2137$ in
T-flange (t) See Table 54	width = 2.6357 in thickness = 0.2362 in	$h_s = 3.5595$ in

Table 9 Summary of stiffened plate model 3 parameters

Configuration	Flange Parameters	Web Parameters
Model 3	$A_f = 0.8113 \text{ in}^2$	$h_w = 3.3233$ in $t_w = 0.2362$ in
No flange See Table 40	No flange area	Same as above
Bulb-flat (b) See Table 44	$t_w = 0.2362$ in $t_{bf} = 0.9843$ in $r = 0.1969$ in $r_1 = (1/10)t_w = 0.0236$ in $\alpha = \pi/6$ radians $h_f = 0.9924$ in	$h_s = 4.3157$ in
Circular (c) See Table 50	radius = 0.5082 in $h_f = 1.0163$ in	$h_s = 4.3396$ in
T-flange (t) See Table 54	width = 3.4343 in = 87.23 mm thickness = 0.2362 in = 6 mm	$h_s = 3.5595$ in

Table 10 Summary of stiffened plate model 4 parameters

Configuration	Flange Parameters	Web Parameters
Model 4	Same as model 1	$h_w = 3.9138$ in $t_w = 0.2362$ in
No flange See Table 41	No flange area	Same as above
Bulb-flat (b) See Table 45	Same as model 1b	$h_s = 4.7244$ in
Circular (c) See Table 51	Same as model 1c	$h_s = 4.7276$ in
T-flange (t) See Table 55	Same as model 1t	$h_s = 4.1501$ in

Table 11 Summary of stiffened plate model 5 parameters

Configuration	Flange Parameters	Web Parameters
Model 5	Same as model 2	$h_w = 3.9138$ in $t_w = 0.2362$ in
No flange See Table 41	No flange area	Same as above
Bulb-flat (b) See Table 46	Same as model 2b	$h_s = 4.7926$ in
Circular (c) See Table 52	Same as model 2c	$h_s = 4.8042$ in
T-flange (t) See Table 55	Same as model 2t	$h_s = 4.1501$ in

Table 12 Summary of stiffened plate model 6 parameters

Configuration	Flange Parameters	Web Parameters
Model 6	Same as model 3	$h_w = 3.9138$ in $t_w = 0.2362$ in
No flange See Table 41	No flange area	Same as above
Bulb-flat (b) See Table 47	Same as model 3b	$h_s = 4.9063$ in
Circular (c) See Table 53	Same as model 3c	$h_s = 4.9301$ in
T-flange (t) See Table 55	Same as model 3t	$h_s = 4.1501$ in

The following tables present intermediate results for the stiffened plate models.

Table 13 Model 1 intermediate results

Result	Bulb-flat	Circular	T-flange
h_f (in)	0.8106	0.8138	0.2362
$\bar{x}$ (in)	0.3214	0.4069	0.1181
$\bar{y}$ (in)	0.3694	0.4069	1.1010
I_c (in^4)	0.0526	0.0431	0.2126
I_{xc} (in^4)	0.0309	0.0215	0.2102
J_f (in^4)	0.0321	0.0431	0.0090
I_f (in^4)	0.2100	0.1292	0.2199
EI_{xc} (lb-in^2)	926071	645945	6305666
GJ_f (lb-in^2)	370796	496881	104091
Mode 1 (psi)	35599	36107	34548
Mode 2 (psi)	29053	28905	31902
Mode 3 (psi)	29356	29455	35105

Table 14 Model 2 intermediate results

Result	Bulb-flat	Circular	T-flange
h_f (in)	0.8788	0.8904	0.2362
$\bar{x}$ (in)	0.3413	0.4452	0.1181
$\bar{y}$ (in)	0.4145	0.4452	1.3179
I_c (in^4)	0.0773	0.0617	0.3633
I_{xc} (in^4)	0.0473	0.0308	0.3604
J_f (in^4)	0.0449	0.0617	0.0109
I_f (in^4)	0.3119	0.1851	0.3720
EI_{xc} (lb-in^2)	1417646	925443	10813397
GJ_f (lb-in^2)	517932	711879	126078
Mode 1 (psi)	36164	36946	34614
Mode 2 (psi)	29261	29001	34229
Mode 3 (psi)	30474	30553	40794

Table 15 Model 3 intermediate results

Result	Bulb-flat	Circular	T-flange
h_f (in)	0.9924	1.0163	0.2362
$\overline{x}$ (in)	0.3753	0.5082	0.1181
$\overline{y}$ (in)	0.4886	0.5082	1.7172
I_c (in^4)	0.1361	0.1047	0.8011
I_{xc} (in^4)	0.0872	0.0524	0.7974
J_f (in^4)	0.0735	0.1047	0.0144
I_f (in^4)	0.5564	0.3142	0.8125
EI_{xc} (lb-in^2)	2617311	1571197	23921250
GJ_f (lb-in^2)	848126	1208613	166564
Mode 1 (psi)	37428	38882	34713
Mode 2 (psi)	29798	29247	41024
Mode 3 (psi)	33128	33117	57198

Table 16 Model 4 intermediate results

Result	Bulb-flat	Circular	T-flange
h_f (in)	0.8106	0.8138	0.2362
$\overline{x}$ (in)	0.3214	0.4069	0.1181
$\overline{y}$ (in)	0.3694	0.4069	1.1010
I_c (in^4)	0.0526	0.0431	0.2126
I_{xc} (in^4)	0.0309	0.0215	0.2102
J_f (in^4)	0.0321	0.0431	0.0090
I_f (in^4)	0.2100	0.1292	0.2199
EI_{xc} (lb-in^2)	926071	645945	6305666
GJ_f (lb-in^2)	370796	496881	104091
Mode 1 (psi)	34602	35109	33551
Mode 2 (psi)	28862	28657	32783
Mode 3 (psi)	29541	29495	37813

Table 17 Model 5 intermediate results

Result	Bulb-flat	Circular	T-flange
h_f (in)	0.8788	0.8904	0.2362
$\overline{x}$ (in)	0.3413	0.4452	0.1181
$\overline{y}$ (in)	0.4145	0.4452	1.3179
I_c (in^4)	0.0773	0.0617	0.3633
I_{xc} (in^4)	0.0473	0.0308	0.3604
J_f (in^4)	0.0449	0.0617	0.0109
I_f (in^4)	0.3119	0.1851	0.3720
EI_{xc} (lb-in^2)	1417646	925443	10813397
GJ_f (lb-in^2)	517932	711879	126078
Mode 1 (psi)	35166	35947	33618
Mode 2 (psi)	29148	28791	35980
Mode 3 (psi)	30844	30672	45530

Table 18 Model 6 intermediate results

Result	Bulb-flat	Circular	T-flange
h_f (in)	0.9924	1.0163	0.2362
$\overline{x}$ (in)	0.3753	0.5082	0.1181
$\overline{y}$ (in)	0.4886	0.5082	1.7172
I_c (in^4)	0.1361	0.1047	0.8011
I_{xc} (in^4)	0.0872	0.0524	0.7974
J_f (in^4)	0.0735	0.1047	0.0144
I_f (in^4)	0.5564	0.3142	0.8125
EI_{xc} (lb-in^2)	2617311	1571197	23921250
GJ_f (lb-in^2)	848126	1208613	166564
Mode 1 (psi)	36430	37882	33718
Mode 2 (psi)	29886	29129	45307
Mode 3 (psi)	33964	33430	67754

The following pictures show the deflection of the plate and web at the onset of buckling for Model 1b. The plate and web panels buckle in 4 half waves along the longitudinal axis. The bulb-flat flange is not visible, but its properties exist in the curve that defines the top of the web.

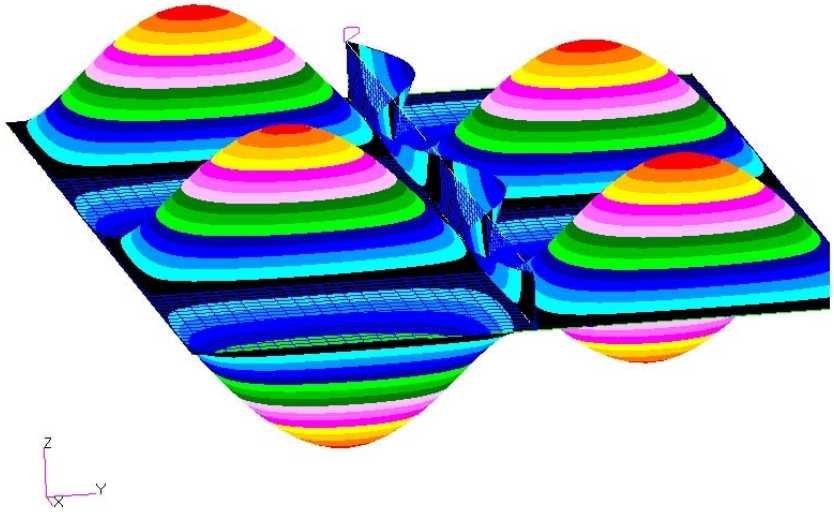

Figure 18 MSC Nastran picture 1 for stiffened plate Model 1b

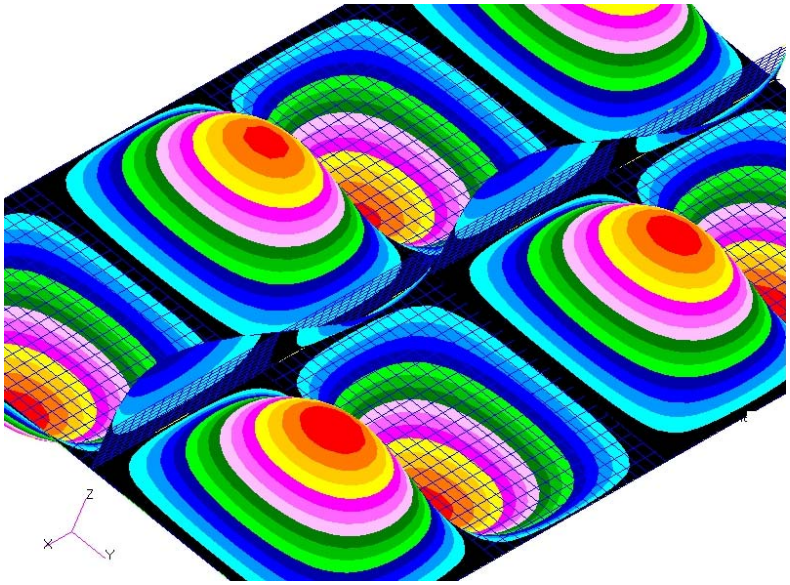

Figure 19 MSC Nastran picture 2 for stiffened plate Model 1b

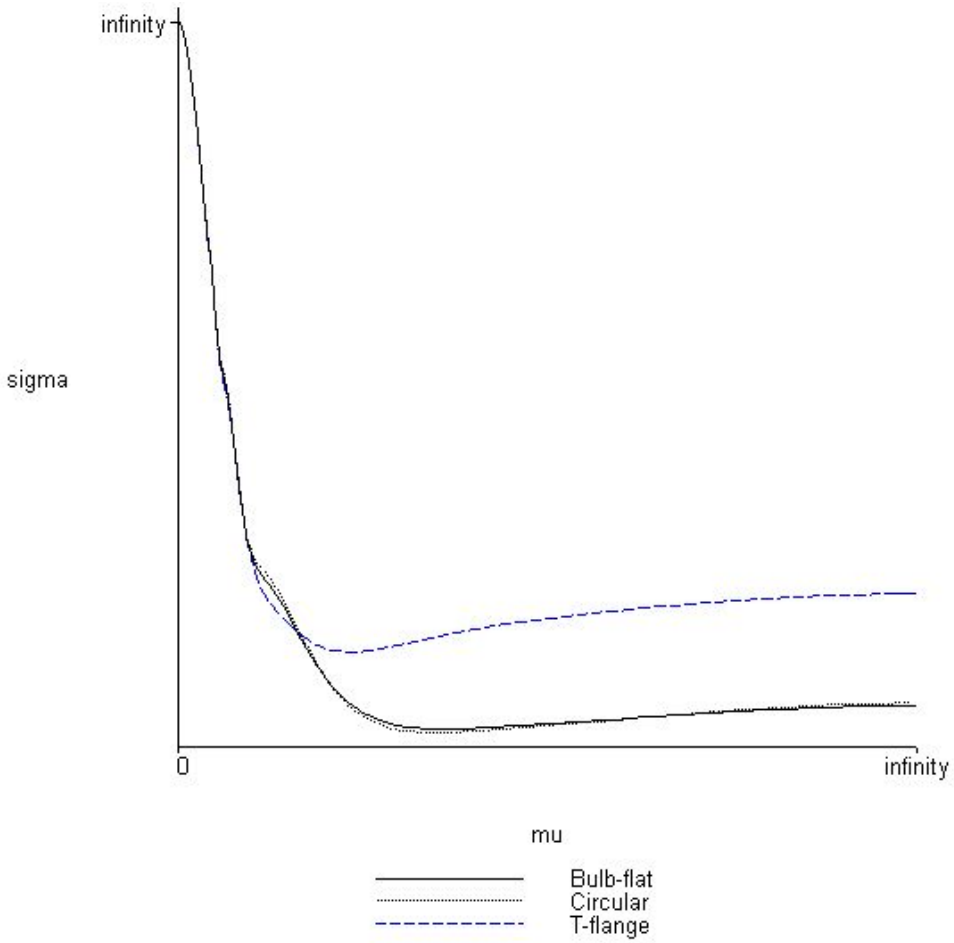

Figure 20 Maple 8 graph 1 of the buckling loads for Model 1

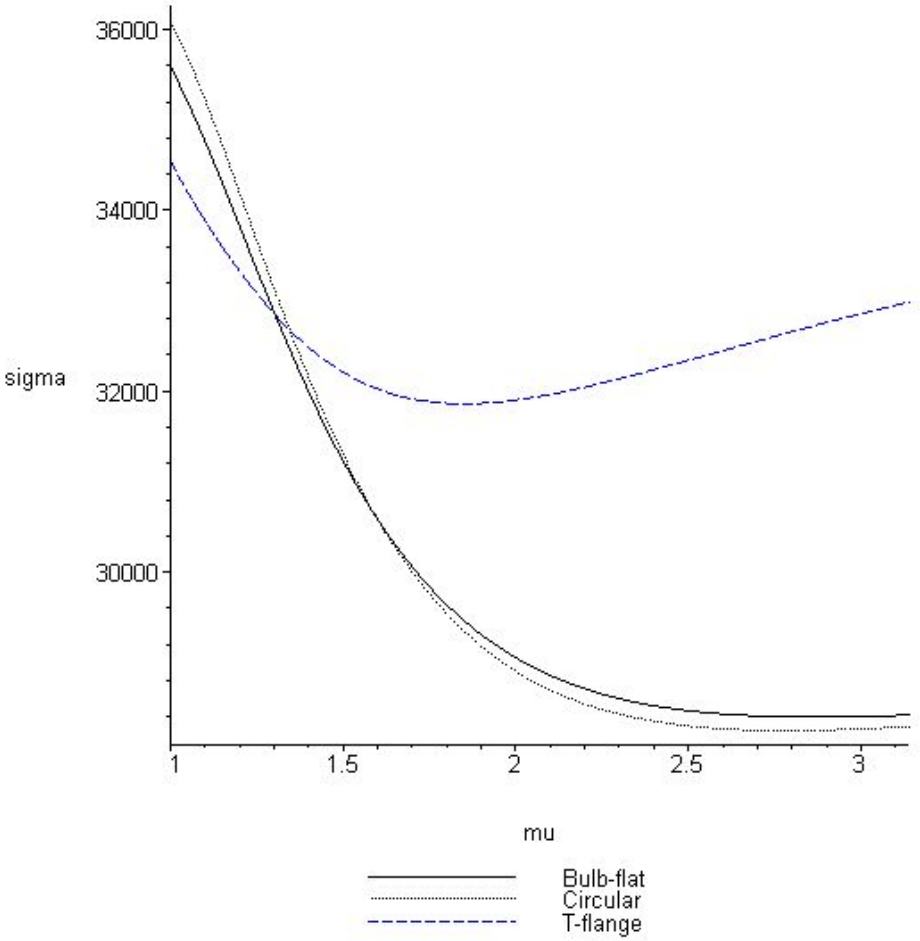

Figure 21 Maple 8 graph 2 of the buckling loads for Model 1

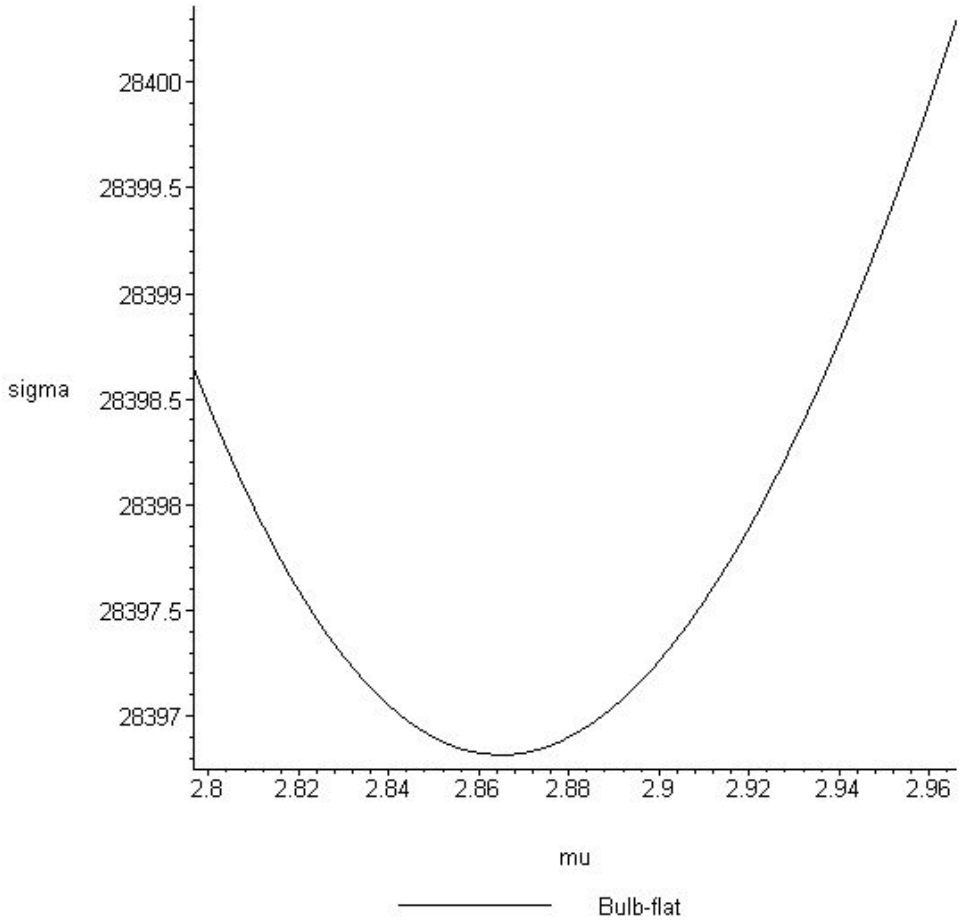

Figure 22 Maple 8 graph of the buckling load for the bulb-flat configuration of Model 1

The pictures below show the difference in the buckling behavior between models 2b and 3b. In each picture, the top of the web has the beam characteristics of a bulb-flat flange. The flange in the left picture has an area property of 0.6226 in^2. The flange in the

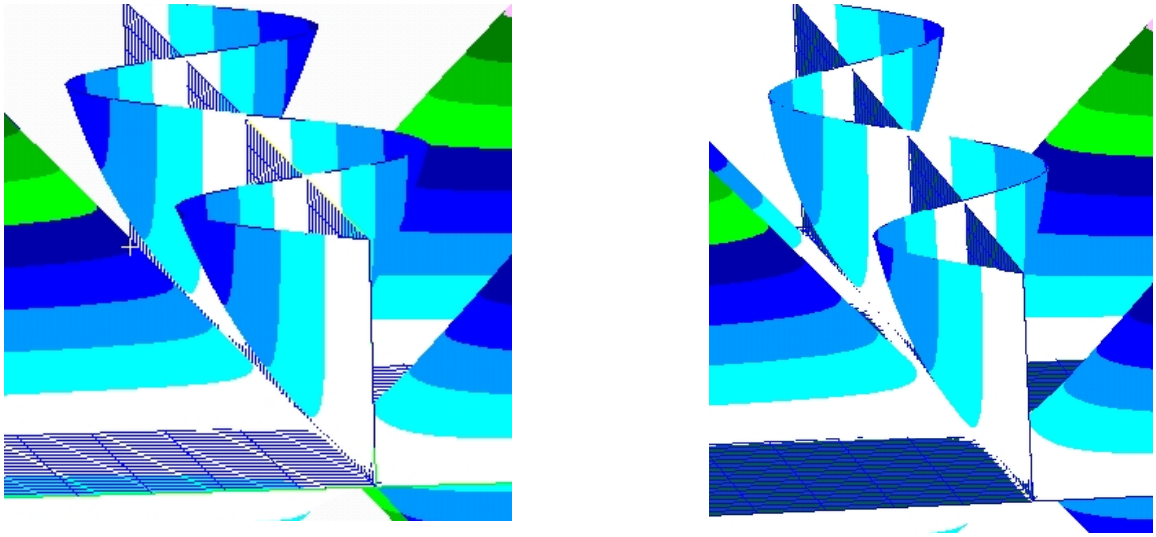

Figure 23 MSC Nastran pictures showing the buckling behavior of the webs with bulb-flat flanges for Models 2b (left) and 3b (right)

right picture has an area property of 0.8113 in^2. These properties are not visible in the pictures, but exist in the curve that defines the top of each web. The web height in both pictures is 3.3233 in. From Table 20, the μ values for the left and right pictures are 2.57 and 2.25 respectively. This indicates there is more lateral bending of the Model 2b flange at the onset of buckling, which agrees with the pictures shown above.

The pictures below show the difference in the buckling behavior between models 4b, 5b, and 6b from left to right respectively. The flanges have area properties of 0.5202 in^2, 0.6226 in^2, and 0.8113 in^2, respectively. The web height in the pictures is 3.9138 in. From Table 20, the μ values are 2.68, 2.40, and 2.11, respectively.

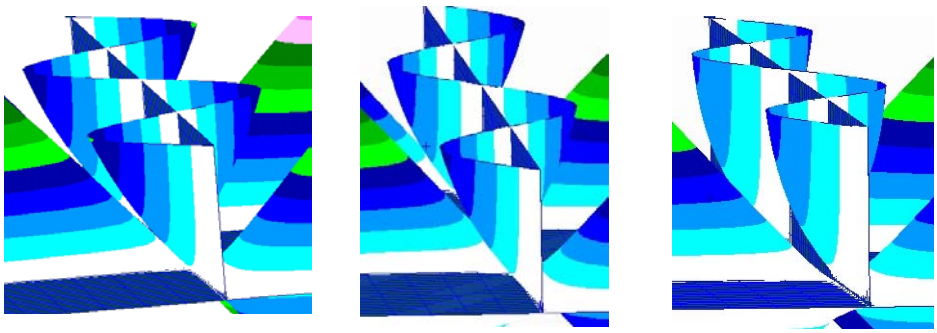

Figure 24 MSC Nastran pictures showing the buckling behavior of the webs with bulb-flat flanges for Models 4b (left), 5b (center), and 6b (right)

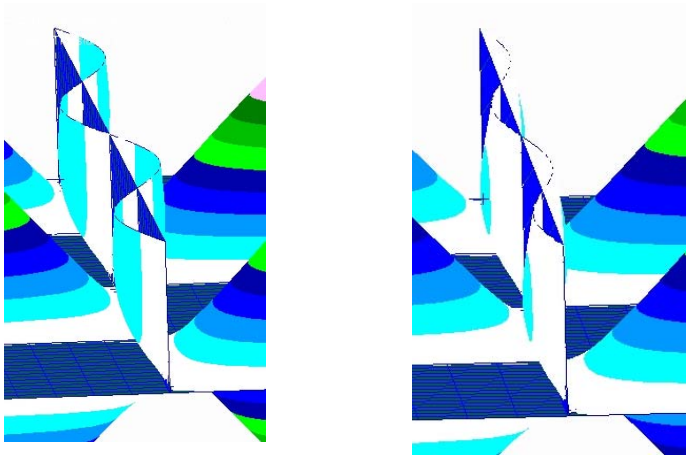

Figure 25 MSC Nastran pictures showing the buckling behavior of the webs with T-flanges for Models 4t (left) and 6t (right)

The pictures above show the difference in the buckling behavior between models 4t and 6t. The flanges have area properties of 0.5202 in^2 and 0.8113 in^2, respectively. The web height in the pictures is 3.9138 in. From Table 22, the μ values are 1.51 and 1.08, respectively.

The following tables show the formula predictions and finite element results.

Table 19 No flange FE results

Model#	FE Results (psi)	Analytic Prediction (psi)	Percent Change
1-3	26928	27181	0.94%
4-6	26892	27138	0.91%

Table 20 Bulb-flat FE results

Model#	FE Results (psi)	Analytic Prediction (psi)	μ	Percent Change
1b	27672	28397	2.86	2.62%
2b	27877	28824	2.57	3.40%
3b	28203	29642	2.25	5.10%
4b	27663	28425	2.68	2.75%
5b	27881	28908	2.40	3.68%
6b	28217	29852	2.11	5.79%

Table 21 Circular FE results

Model#	FE Results (psi)	Analytic Prediction (psi)	μ	Percent Change
1c	27558	28246	2.78	2.50%
2c	27703	28524	2.54	2.96%
3c	27936	29000	2.29	3.81%
4c	27498	28178	2.65	2.47%
5c	27654	28469	2.44	2.95%
6c	27907	28996	2.21	3.90%

Table 22 T-flange FE results

Model#	FE Results (psi)	Analytic Prediction (psi)	μ	Percent Change
1t	28767	31864	1.85	10.77%
2t	29030	33200	1.45	14.36%
3t	29291	34220	1.15	16.83%
4t	28739	32146	1.51	11.85%
5t	28933	32945	1.23	13.87%
6t	29119	33460	1.08	14.91%

Table 19 compares the results for the stiffened plates without flanges. The formula values nearly agree with the finite element results. Table 20 compares the bulb-flat configurations for each model. The formula values are less than 6% above the finite element results. Examination of the μ values indicates that the buckling behavior of the stiffened plates tend to have significant bending of the flange and web with a degree of flange torsion. This type of buckling behavior can be seen in the Nastran pictures on the previous pages. As the flange areas increase between models 1, 2, and 3, and also between models 4, 5, and 6, the μ values tend to approach the value 2, indicating perhaps an increasing torsional rigidity effect. The buckling loads tend to increase as the flange area increases, as expected. Overall, the results indicate that at the onset of buckling, the bulb-flat stiffened plate structures deflect with a combination of flange bending and torsion along with web bending. Table 21 compares the circular flange configurations, which appear to buckle at a slightly lower value than the bulb-flat configurations, but behave similar to them at the onset of buckling. Table 22 compares the T-flange configurations. From the finite element results, the buckling load of a plate with a bulb-flat stiffener is 3% - 4% less than that of a plate with a T-flange stiffener with the same cross-sectional area. Based on the μ values for the T-flange configuration, bending of the flange tends to decrease as the cross-sectional area increases. The difference in the formula values from the finite element values could be due to fundamental assumption (ix). Though the T-flange is solid, treating the flange as a thin web plate strip instead of a beam may achieve more accurate predictions. This may explain the increase in error for the bulb-flat and T-flange cases as the area increases due to flange widening. The increasing error is less pronounced for the circular flange models.

THIS PAGE INTENTIONALLY LEFT BLANK

IV. FINDINGS AND CONCLUSIONS

The following summarizes the major findings and conclusions of this work. Each major finding or conclusion is stated followed by explanatory comments.

- Determined cross-sectional boundary equations for the bulb-flat flange cross-section.

In order to conduct an accurate analysis of the bulb-flat cross-section, it is necessary to determine equations that define or at least approximate the boundary that is a closed bounded plane region. The equation that defines the boundary of a simple geometric cross-section like a circle or ellipse is well known. The boundary equation for uncommon and asymmetric cross-sections is often very difficult to define. As a result of this study, functions exist that define the boundary of the bulb-flat flange cross-section.

- Derived planar property value expressions.

Determining the critical buckling load of a stiffened plate structure requires knowledge of several planar property values of the plate's cross-section. Based on the boundary equations and the application of multivariable calculus, the double integral provides expressions for calculating the various planar properties of the bulb-flat flange cross-section. Though the integral expressions are complicated, they could be simplified by assigning fixed values to certain variables.

- Determined an approximate torsional constant expression that is more accurate than idealizing.

The Saint-Venant torsional constant is one of the key property values involved in the analysis of stiffened plate structures. Due to the uncommon shape and asymmetrical property of the bulb-flat cross-section, determining the exact expression for the Saint-Venant torsional constant is difficult and does not exist in published literature. As a result of this study, an approximate expression exists for the Saint-Venant torsional constant of a specified class of bulb-flat cross-sections. The approximate expression is a one-term function relating the cross-sectional area to the polar moment of inertia. The

approximate expression is more accurate than the estimate obtained by idealizing the cross-section as an angle flange.

- Demonstrated that the torsional property of the bulb-flat stiffener is better than previously understood. The torque-carrying capacity of a bulb-flat stiffener (possessing no structural flaws) is greater than that of an area-equivalent angle stiffener.

In previous investigations the torsional nature of the bulb-flat stiffener was idealized as an angle flange stiffener. That is, the bulb-flat flange cross-section was treated like a rectangular cross-section in regards to the torsional and warping properties. Such treatment imputed error in the calculation of the bulb-flat stiffener's torsional rigidity resulting in conservative estimates. Finite element analysis indicates that the torque-carrying capacity of a bulb-flat stiffener (possessing no structural flaws) is greater than that of an area-equivalent angle stiffener.

- Derived a general expression to predict the buckling load due to the stiffener tripping of a simply supported rectangular stiffened plate subjected to axial compression. In the investigation, the predicted value is less than 6% higher than the finite element result.

Understanding the elastic stability of stiffened plate structures is important to the analyst, designer, and educator involved in the analysis and design of structures. Use of the energy method provides a technique to derive a general expression for the buckling load due to the stiffener tripping of a simply supported rectangular stiffened plate subjected to axial compression. As a result of this study, a useful analytic expression exists that allows the user to predict the critical buckling load and the buckling behavior of a stiffened plate at the onset of stiffener tripping. The onset of stiffener tripping negates the stiffener's support to the plate panel and leads to eventual collapse of the structure. The general expression involves a constant called μ that is determined graphically. The value of μ can be interpreted to indicate the deflection behavior based on three special deflection modes.

Mode	μ	Flange bending	Flange torsion	Web bending
1	1	No	Yes	Yes
2	2	Yes	No	Yes
3	∞	Yes	Yes	No

Finite element analyses of several stiffened plate models is presented to validate the analytic expressions and assess the sensitivity of the formulas to factor variability. Knowledge of MSC Nastran/Patran software and finite element principles along with the Maple 8 computer environment was essential for this investigation.

- Demonstrated that the buckling behavior of the bulb-flat stiffened plate is markedly unlike that of the T-flange configuration. The bulb-flat tends to buckle more laterally and have a lower buckling load value than an area-equivalent T-flange stiffened plate.

The bulb-flat stiffened plate tends to buckle in a Mode 2 fashion, while the T-flange stiffened plate tends to buckle in a Mode 1 fashion. Hence, the torsional superior bulb-flat tends to bend laterally at the onset of stiffener tripping, while the flexural superior T-flange tends to twist axially at the onset of stiffener tripping.

As a result of this investigation, several essential future research directions exist. Future research should include:

- Investigating methods to determine the μ value by other than graphical means.
- Investigating the use of conformal mapping to determine the exact expression for the bulb-flat torsional constant.
- Investigating solutions to the torsion problem for asymmetric cross-sections.
- Conducting investigations of other flange cross-sections, multiple stiffener configurations, and grillages.
- Conducting further investigations of the T flange by treating the flange as a thin web plate strip instead of a beam. This treatment may achieve more accurate predictions for the T-flange buckling loads.
- Developing algorithms that increase efficiency in stiffened plate analysis and design.

THIS PAGE INTENTIONALLY LEFT BLANK

APPENDIX A. THE BULB-FLAT FLANGE HEIGHT FORMULA

This appendix presents the derivation of the formula for the height of the bulb-flat flange cross-section. Maple 8 computer environment software was used to derive some of the formula final forms. Five independent variables uniquely determine a specific bulb-flat cross-section.

t_w	Thickness of the web (length)
t_{bf}	Thickness of the flange bulb (length)
r	Radius of curvature of flange bulb and neck curve (length)
r_1	Radius of curvature of the cross-section corner (length)
α	Slope angle of the flange neck (radians)

It will be shown that only three of the independent variables, t_{bf}, r and α, determine the height of the flange. Throughout this discussion, it is assumed $0 < \alpha < \pi/2$. The following figures show a model of the bulb-flat flange oriented horizontally with the bulb extended to one side of the web.

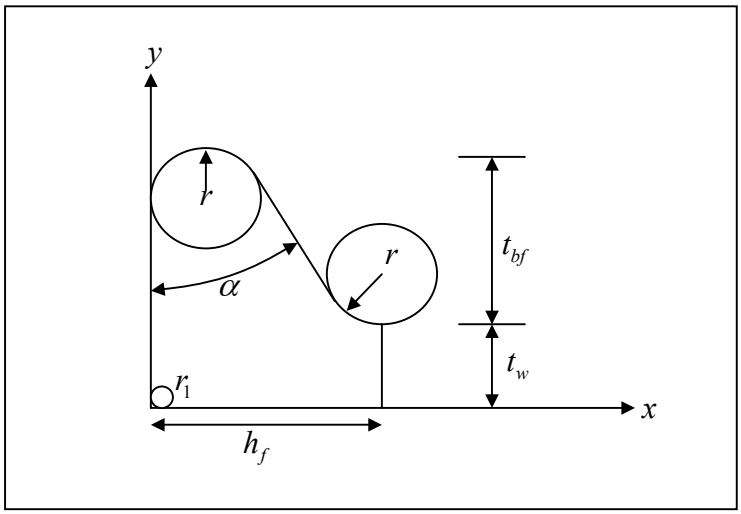

Figure 26 Bulb-flat flange geometry

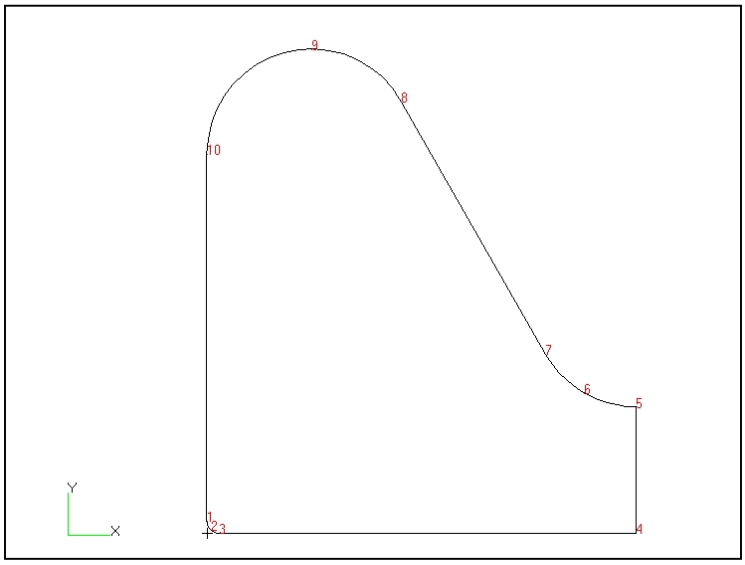

Figure 27 MSC Patran Bulb-flat flange boundary points for cross-section properties

The three circles in Figure 26 show the radii of curvature at the corners of the flange. The height of the flange, denoted h_f, is the distance from the left boundary $x = 0$ to the right boundary $x = h_f$. Consider the line segment tangent to the two circles of radius r. In Figure 27, the line segment connects point 7 (x_7, y_7) and point 8 (x_8, y_8) where

$$\begin{aligned} &x_7 \text{ is to be determined} \\ &y_7 = t_w + r - r\sin\alpha \end{aligned} \tag{69}$$

and

$$\begin{aligned} x_8 &= r + r\cos\alpha \\ y_8 &= t_w + t_{bf} - r + r\sin\alpha \end{aligned} \tag{70}$$

The flange height can be expressed simply as

$$h_f = x_7 + r\cos\alpha \tag{71}$$

Once x_7 is determined, h_f is determined from (71). The slope of line segment is

$$slope = \frac{\Delta y}{\Delta x} = \frac{y_7 - y_8}{x_7 - x_8} = -\cot\alpha \qquad \Rightarrow \qquad x_7 = -\left(y_7 - y_8\right)\tan\alpha + x_8 \tag{72}$$

From (69) and (70)

$$\begin{aligned} y_7 - y_8 &= \left(t_w + r - r\sin\alpha\right) - \left(t_w + t_{bf} - r + r\sin\alpha\right) \\ &= -t_{bf} + 2r\left(1 - \sin\alpha\right) \end{aligned} \tag{73}$$

From (72) and (73)

$$x_7 - x_8 = t_{bf}\tan\alpha - 2r\tan\alpha + 2r\sec\alpha - 2r\cos\alpha \tag{74}$$

and

$$x_7 = t_{bf}\tan\alpha + r - 2r\tan\alpha + 2r\sec\alpha - r\cos\alpha \tag{75}$$

Substituting (75) into (71) yields the following formula.

$$h_f = t_{bf}\tan\alpha + r\left(1 - 2\tan\alpha + 2\sec\alpha\right) \tag{76}$$

THIS PAGE INTENTIONALLY LEFT BLANK

APPENDIX B. THE PLANAR PROPERTY FORMULAS

The purpose of this appendix is to present the derivation of the planar property formulas for the bulb-flat flange. It is assumed $0<\alpha<\pi/2$ throughout the discussion.

Let the closed bounded plane region R be defined by $0\le x\le h_f$, $g(x)\le y\le f(x)$, with $f(x)$ and $g(x)$ on $x\in\left[0,h_f\right]$, such that

$$f\left(x\right)=\begin{cases} f_1\left(x\right)=\left(t_w+t_{bf}-r\right)+\sqrt{r^2-\left(x-r\right)^2}, & 0\le x<r+r\cos\alpha \\ f_2\left(x\right)=mx+b, & r+r\cos\alpha\le x<h_f-r\cos\alpha \\ f_3\left(x\right)=\left(t_w+r\right)-\sqrt{r^2-\left(x-h_f\right)^2}, & h_f-r\cos\alpha\le x\le h_f \end{cases} \tag{77}$$

and

$$g\left(x\right)=\begin{cases} g_1\left(x\right)=r_1-\sqrt{r_1^2-\left(x-r_1\right)^2}, & 0\le x<r_1 \\ g_2\left(x\right)=0, & r_1\le x\le h_f \end{cases} \tag{78}$$

where

$$\begin{aligned} m&=-\cot\alpha \\ b&=t_w+t_{bf}+r\left(\cot\alpha+\csc\alpha-1\right) \\ h_f&=t_{bf}\tan\alpha+r\left(1-2\tan\alpha+2\sec\alpha\right) \end{aligned} \tag{79}$$

By the theorem of integrability of a piecewise function[8], since f and g are piecewise defined functions on the same closed interval, then f and g are integrable on the same closed interval. The planar property formulas can be determined from the following expression where m,n are nonnegative integers.

$$\iint_R x^m y^n dA=\int_0^{h_f}\int_{g(x)}^{f(x)} x^m y^n dydx=\frac{1}{n+1}\int_0^{h_f} x^m\left\{\left[f\left(x\right)\right]^{n+1}-\left[g\left(x\right)\right]^{n+1}\right\}dx$$

[8] Ross, K.A., Elementary Analysis: *The Theory of Calculus*, Springer, New York, pp. 258-259.

$$\iint_R x^m y^n dA = \frac{1}{n+1}\int_{-\frac{\pi}{2}}^{\frac{\pi}{2}-\alpha} \left(r + r\sin\theta\right)^m \left(t_w + t_{bf} - r + r\cos\theta\right)^{n+1} r\cos\theta\, d\theta$$
$$+ \frac{1}{n+1}\int_{r+r\cos\alpha}^{h_f - r\cos\alpha} x^m \left(-x\cot\alpha + t_w + t_{bf} + r\cot\alpha + r\csc\alpha - r\right)^{n+1} dx$$
$$+ \frac{1}{n+1}\int_{\alpha-\frac{\pi}{2}}^{0} \left(h_f + r\sin\theta\right)^m \left(t_w + r - r\cos\theta\right)^{n+1} r\cos\theta\, d\theta$$
$$- \frac{1}{n+1} r_1^{m+n+2}\int_{-\frac{\pi}{2}}^{0} \left(1+\sin\theta\right)^m \left(1-\cos\theta\right)^{n+1} \cos\theta\, d\theta$$

where

$$h_f = t_{bf}\tan\alpha + r\left(1 - 2\tan\alpha + 2\sec\alpha\right)$$
$$0 < \alpha < \frac{\pi}{2}, \quad -\frac{\pi}{2} \le \theta \le \frac{\pi}{2}, \quad 0 \le x \le h_f$$

By definition, the area of the closed bounded plane region R is the value of the integral

$$\text{Area} = \iint_R x^0 y^0\, dA = \iint_R dA = \int_0^{h_f}\int_{g(x)}^{f(x)} dy\, dx = \int_0^{h_f} f(x) - g(x)\, dx$$

Hence,

$$\iint_R dA = \int_0^{r+r\cos\alpha} f_1(x)\, dx + \int_{r+r\cos\alpha}^{h_f - r\cos\alpha} f_2(x)\, dx + \int_{h_f - r\cos\alpha}^{h_f} f_3(x)\, dx - \int_0^{r_1} g_1(x)\, dx - \int_{r_1}^{h_f} g_2(x)\, dx$$

$$\iint_R dA = \int_{-\frac{\pi}{2}}^{\frac{\pi}{2}-\alpha} \left(t_w + t_{bf} - r + r\cos\theta\right) r\cos\theta\, d\theta + \int_{r+r\cos\alpha}^{h_f - r\cos\alpha} \left(-x\cot\alpha + t_w + t_{bf} + r\cot\alpha + r\csc\alpha - r\right) dx$$
$$+ \int_{\alpha-\frac{\pi}{2}}^{0} \left(t_w + r - r\cos\theta\right) r\cos\theta\, d\theta - r_1^2 \int_{-\frac{\pi}{2}}^{0} \left(1-\cos\theta\right)\cos\theta\, d\theta$$

Integrating and collecting terms yields the area of the bulb-flat flange:

$$A_f = -\left(1 - \frac{\pi}{4}\right)\left(r^2 + r_1^2\right) + rt_w\left(1 - 2\tan\alpha + 2\sec\alpha\right) + rt_{bf}\left(1 - \tan\alpha + \sec\alpha\right)$$
$$+ \frac{1}{2}t_{bf}^{\,2}\tan\alpha + t_w t_{bf}\tan\alpha \qquad (80)$$

Other planar property formulas are determined in similar fashion and are summarized below (algebraic expansion omitted).

$$
\begin{aligned}
M_x &= \iint_R x^0 y^1 dA = \iint_R y\, dA \\
&= \frac{1}{2}\int_{-\frac{\pi}{2}}^{\frac{\pi}{2}-\alpha} \left(t_w + t_{bf} - r + r\cos\theta\right)^2 r\cos\theta\, d\theta \\
&+ \frac{1}{2}\int_{r+r\cos\alpha}^{h_f - r\cos\alpha} \left(-x\cot\alpha + t_w + t_{bf} + r\cot\alpha + r\csc\alpha - r\right)^2 dx \\
&+ \frac{1}{2}\int_{\alpha-\frac{\pi}{2}}^{0} \left(t_w + r - r\cos\theta\right)^2 r\cos\theta\, d\theta - \frac{1}{2} r_1^3 \int_{-\frac{\pi}{2}}^{0} \left(1-\cos\theta\right)^2 \cos\theta\, d\theta
\end{aligned}
\tag{81}
$$

$$
\begin{aligned}
M_y &= \iint_R x^1 y^0 dA = \iint_R x\, dA \\
&= \int_{-\frac{\pi}{2}}^{\frac{\pi}{2}-\alpha} \left(r + r\sin\theta\right)\left(t_w + t_{bf} - r + r\cos\theta\right) r\cos\theta\, d\theta \\
&+ \int_{r+r\cos\alpha}^{h_f - r\cos\alpha} x\left(-x\cot\alpha + t_w + t_{bf} + r\cot\alpha + r\csc\alpha - r\right) dx \\
&+ \int_{\alpha-\frac{\pi}{2}}^{0} \left(h_f + r\sin\theta\right)\left(t_w + r - r\cos\theta\right) r\cos\theta\, d\theta - r_1^3 \int_{-\frac{\pi}{2}}^{0} \left(1+\sin\theta\right)\left(1-\cos\theta\right)\cos\theta\, d\theta
\end{aligned}
\tag{82}
$$

$$
\bar{x} = \frac{M_y}{A_f} \tag{83}
$$

$$
\bar{y} = \frac{M_x}{A_f} \tag{84}
$$

$$
\begin{aligned}
I_{xx} &= \iint_R x^0 y^2 dA = \iint_R y^2 \, dA \\
&= \frac{1}{3} \int_{-\frac{\pi}{2}}^{\frac{\pi}{2}-\alpha} \left(t_w + t_{bf} - r + r\cos\theta\right)^3 r\cos\theta \, d\theta \\
&+ \frac{1}{3} \int_{r+r\cos\alpha}^{h_f - r\cos\alpha} \left(-x\cot\alpha + t_w + t_{bf} + r\cot\alpha + r\csc\alpha - r\right)^3 dx \\
&+ \frac{1}{3} \int_{\alpha-\frac{\pi}{2}}^{0} \left(t_w + r - r\cos\theta\right)^3 r\cos\theta \, d\theta - \frac{1}{3} r_1^4 \int_{-\frac{\pi}{2}}^{0} \left(1-\cos\theta\right)^3 \cos\theta \, d\theta
\end{aligned}
\tag{85}
$$

$$
\begin{aligned}
I_{yy} &= \iint_R x^2 y^0 dA = \iint_R x^2 \, dA \\
&= \int_{-\frac{\pi}{2}}^{\frac{\pi}{2}-\alpha} \left(r + r\sin\theta\right)^2 \left(t_w + t_{bf} - r + r\cos\theta\right) r\cos\theta \, d\theta \\
&+ \int_{r+r\cos\alpha}^{h_f - r\cos\alpha} x^2 \left(-x\cot\alpha + t_w + t_{bf} + r\cot\alpha + r\csc\alpha - r\right) dx \\
&+ \int_{\alpha-\frac{\pi}{2}}^{0} \left(h_f + r\sin\theta\right)^2 \left(t_w + r - r\cos\theta\right) r\cos\theta \, d\theta - r_1^4 \int_{-\frac{\pi}{2}}^{0} \left(1+\sin\theta\right)^2 \left(1-\cos\theta\right)\cos\theta \, d\theta
\end{aligned}
\tag{86}
$$

$$
\begin{aligned}
I_{xy} &= \iint_R x^1 y^1 dA = \iint_R xy \, dA \\
&= \frac{1}{2} \int_{-\frac{\pi}{2}}^{\frac{\pi}{2}-\alpha} \left(r + r\sin\theta\right)\left(t_w + t_{bf} - r + r\cos\theta\right)^2 r\cos\theta \, d\theta \\
&+ \frac{1}{2} \int_{r+r\cos\alpha}^{h_f - r\cos\alpha} x\left(-x\cot\alpha + t_w + t_{bf} + r\cot\alpha + r\csc\alpha - r\right)^2 dx \\
&+ \frac{1}{2} \int_{\alpha-\frac{\pi}{2}}^{0} \left(h_f + r\sin\theta\right)\left(t_w + r - r\cos\theta\right)^2 r\cos\theta \, d\theta \\
&- \frac{1}{2} r_1^4 \int_{-\frac{\pi}{2}}^{0} \left(1+\sin\theta\right)\left(1-\cos\theta\right)^2 \cos\theta \, d\theta
\end{aligned}
\tag{87}
$$

$$
I_{xc} = I_{xx} - A_f \bar{y}^2 \tag{88}
$$

$$I_{yc} = I_{yy} - A_f \overline{x}^2 \tag{89}$$

$$I_{xyc} = I_{xy} - A_f \overline{x}\,\overline{y} \tag{90}$$

$$I_c = I_{xc} + I_{yc} \tag{91}$$

THIS PAGE INTENTIONALLY LEFT BLANK

APPENDIX C. DATA TABLES

This appendix presents flange, stiffener, and plate data tables used to model the cross-sections for finite element analysis. When creating a finite element model of a structure, a matrix represents the structure. The information in the left portion of each table list parameters or references related to the set of points contained in the right portion of the table.

1. DATA FOR BULB-FLAT FLANGE CROSS-SECTION

See Figure 3 and Figure 5.

Table 23 Data for Flange Model 1 in Table 2 (units in mm)

$t_w = 6$ $t_{bf} = 17$ $r = 5$ $r_1 = (1/10)t_w$=6/10 $\alpha = \pi / 6$ $h_f = 20.59$ $A_f = 335.59$	[0.0000 0.6000 0.0000][0.1757 0.1757 0.0000][0.6000 0.0000 0.0000][20.5885 0.0000 0.0000][20.5885 6.0000 0.0000][18.0885 6.6699 0.0000][16.2583 8.5000 0.0000][9.3301 20.5000 0.0000][5.0000 23.0000 0.0000][0.0000 18.0000 0.0000]

Table 24 Data for Flange Model 3 in Table 2 (units in mm)

$t_w = 8$ $t_{bf} = 17$ $r = 5$ $r_1 = (1/10)t_w$=8/10 $\alpha = \pi / 6$ $h_f = 20.59$ $A_f = 376.71$	[0.0000 0.8000 0.0000][0.2343 0.2343 0.0000][0.8000 0.0000 0.0000][20.5885 0.0000 0.0000][20.5885 8.0000 0.0000][18.0885 8.6699 0.0000][16.2583 10.5000 0.0000][9.3301 22.5000 0.0000][5.0000 25.0000 0.0000][0.0000 20.0000 0.0000]

Table 25 Data for Flange Model 5 in Table 2 (units in mm)

$t_w = 7$ $t_{bf} = 19$ $r = 5.5$ $r_1 = (1/10)t_w$=7/10 $\alpha = \pi / 6$ $h_f = 22.82$ $A_f = 422.19$	[0.0000 0.7000 0.0000][0.2050 0.2050 0.0000][0.7000 0.0000 0.0000][22.8205 0.0000 0.0000][22.8205 7.0000 0.0000][20.0705 7.7369 0.0000][18.0574 9.7500 0.0000][10.2631 23.2500 0.0000][5.5000 26.0000 0.0000][0.0000 20.5000 0.0000]

Table 26 Data for Flange Model 7 in Table 2 (units in mm)

$t_w = 10$ $t_{bf} = 19$ $r = 5.5$ $r_1 = (1/10)t_w$=10/10=1 $\alpha = \pi / 6$ $h_f = 22.82$ $A_f = 490.54$	[0.0000 1.0000 0.0000][0.2929 0.2929 0.0000][1.0000 0.0000 0.0000][22.8205 0.0000 0.0000][22.8205 10.0000 0.0000][20.0705 10.7369 0.0000][18.0574 12.7500 0.0000][10.2631 26.2500 0.0000][5.5000 29.0000 0.0000][0.0000 23.5000 0.0000]

Table 27 Data for Flange Model 8 in Table 2 (units in mm)

$t_w = 7$ $t_{bf} = 22$ $r = 6$ $r_1 = (1/10)t_w$=7/10 $\alpha = \pi / 6$ $h_f = 25.63$ $A_f = 519.51$	[0.0000 0.7000 0.0000][0.2050 0.2050 0.0000][0.7000 0.0000 0.0000][25.6299 0.0000 0.0000][25.6299 7.0000 0.0000][22.6299 7.8038 0.0000][20.4338 10.0000 0.0000][11.1962 26.0000 0.0000][6.0000 29.0000 0.0000][0.0000 23.0000 0.0000]

Table 28 Data for Flange Model 10 in Table 2 (units in mm)

$t_w = 9$ $t_{bf} = 22$ $r = 6$ $r_1 = (1/10)t_w$=9/10 $\alpha = \pi / 6$ $h_f = 25.63$ $A_f = 570.70$	[0.0000 0.9000 0.0000][0.2636 0.2636 0.0000][0.9000 0.0000 0.0000][25.6299 0.0000 0.0000][25.6299 9.0000 0.0000][22.6299 9.8038 0.0000][20.4338 12.0000 0.0000][11.1962 28.0000 0.0000][6.0000 31.0000 0.0000][0.0000 25.0000 0.0000]

Table 29 Data for Flange Model 12 in Table 2 (units in mm)

$t_w = 8$ $t_{bf} = 25$ $r = 7$ $r_1 = (1/10)t_w$=8/10 $\alpha = \pi / 6$ $h_f = 29.52$ $A_f = 681.94$	[0.0000 0.8000 0.0000][0.2343 0.2343 0.0000][0.8000 0.0000 0.0000][29.5167 0.0000 0.0000][29.5167 8.0000 0.0000][26.0167 8.9378 0.0000][23.4545 11.5000 0.0000][13.0622 29.5000 0.0000][7.0000 33.0000 0.0000][0.0000 26.0000 0.0000]

Table 30 Data for Flange Model 14 in Table 2 (units in mm)

$t_w = 10$ $t_{bf} = 25$ $r = 7$ $r_1 = (1/10)t_w$=10/10=1 $\alpha = \pi / 6$ $h_f = 29.52$ $A_f = 740.89$	[0.0000 1.0000 0.0000][0.2929 0.2929 0.0000][1.0000 0.0000 0.0000][29.5167 0.0000 0.0000][29.5167 10.0000 0.0000][26.0167 10.9378 0.0000][23.4545 13.5000 0.0000][13.0622 31.5000 0.0000][7.0000 35.0000 0.0000][0.0000 28.0000 0.0000]

2. DATA FOR THE BULB-FLAT STIFFENER CROSS-SECTION

See Figure 1, Figure 7, and Figure 8.

Table 31 Data for first stiffener in Table 5 (units in mm)

$h_s = 120$ $h_f = 20.59$ $h_w = 99.41$ $t_w = 6$ $t_{bf} = 17$ $r = 5$ $r_1 = (1/10)t_w$=6/10 $\alpha = \pi / 6$	[0.0000 0.0000 0.0000][6.0000 0.0000 0.0000][6.0000 99.4115 0.0000][6.6699 101.9115 0.0000][8.5000 103.7417 0.0000][20.5000 110.6699 0.0000][23.0000 115.0000 0.0000][18.0000 120.0000 0.0000][0.6000 120.0000 0.0000][0.1757 119.8243 0.0000][0.0000 119.4000 0.0000]

Table 32 Data for second stiffener in Table 5 (units in mm)

$h_s = 120$ $h_f = 20.59$ $h_w = 99.41$ $t_w = 8$ $t_{bf} = 17$ $r = 5$ $r_1 = (1/10)t_w$=8/10 $\alpha = \pi / 6$	[0.0000 0.0000 0.0000][8.0000 0.0000 0.0000][8.0000 99.4115 0.0000][8.6699 101.9115 0.0000][10.5000 103.7417 0.0000][22.5000 110.6699 0.0000][25.0000 115.0000 0.0000][20.0000 120.0000 0.0000][0.8000 120.0000 0.0000][0.2343 119.7657 0.0000][0.0000 119.2000 0.0000]

Table 33 Data for third stiffener in Table 5 (units in mm)

$h_s = 140$ $h_f = 22.82$ $h_w = 117.18$ $t_w = 7$ $t_{bf} = 19$ $r = 5.5$ $r_1 = (1/10)t_w$=7/10 $\alpha = \pi / 6$	[0.0000 0.0000 0.0000][7.0000 0.0000 0.0000][7.0000 117.1795 0.0000][7.7369 119.9295 0.0000][9.7500 121.9426 0.0000][23.2500 129.7369 0.0000][26.0000 134.5000 0.0000][20.5000 140.0000 0.0000][0.7000 140.0000 0.0000][0.2050 139.7950 0.0000][0.0000 139.3000 0.0000]

Table 34 Data for fourth stiffener in Table 5 (units in mm)

$h_s = 140$ $h_f = 22.82$ $h_w = 117.18$ $t_w = 10$ $t_{bf} = 19$ $r = 5.5$ $r_1 = (1/10)t_w$=10/10=1 $\alpha = \pi / 6$	[0.0000 0.0000 0.0000][10.0000 0.0000 0.0000][10.0000 117.1795 0.0000][10.7369 119.9295 0.0000][12.7500 121.9426 0.0000][26.2500 129.7369 0.0000][29.0000 134.5000 0.0000][23.5000 140.0000 0.0000][1.0000 140.0000 0.0000][0.2929 139.7071 0.0000][0.0000 139.0000 0.0000]

Table 35 Data for fifth stiffener inTable 5 (units in mm)

$h_s = 160$ $h_f = 25.63$ $h_w = 134.37$ $t_w = 7$ $t_{bf} = 22$ $r = 6$ $r_1 = (1/10)t_w$=7/10 $\alpha = \pi / 6$	[0.0000 0.0000 0.0000][7.0000 0.0000 0.0000][7.0000 134.3701 0.0000][7.8038 137.3701 0.0000][10.0000 139.5662 0.0000][26.0000 148.8038 0.0000][29.0000 154.0000 0.0000][23.0000 160.0000 0.0000][0.7000 160.0000 0.0000][0.2050 159.7950 0.0000][0.0000 159.3000 0.0000]

Table 36 Data for sixth stiffener in Table 5 (units in mm)

$h_s = 160$ $h_f = 25.63$ $h_w = 134.37$ $t_w = 9$ $t_{bf} = 22$ $r = 6$ $r_1 = (1/10)t_w$=9/10 $\alpha = \pi / 6$	[0.0000 0.0000 0.0000][9.0000 0.0000 0.0000][9.0000 134.3701 0.0000][9.8038 137.3701 0.0000][12.0000 139.5662 0.0000][28.0000 148.8038 0.0000][31.0000 154.0000 0.0000][25.0000 160.0000 0.0000][0.9000 160.0000 0.0000][0.2636 159.7364 0.0000][0.0000 159.1000 0.0000]

Table 37 Data for seventh stiffener in Table 5 (units in mm)

$h_s = 180$ $h_f = 29.52$ $h_w = 150.48$ $t_w = 8$ $t_{bf} = 25$ $r = 7$ $r_1 = (1/10)t_w$=8/10 $\alpha = \pi / 6$	[0.0000 0.0000 0.0000][8.0000 0.0000 0.0000][8.0000 150.4833 0.0000][8.9378 153.9833 0.0000][11.5000 156.5455 0.0000][29.5000 166.9378 0.0000][33.0000 173.0000 0.0000][26.0000 180.0000 0.0000][0.8000 180.0000 0.0000][0.2343 179.7657 0.0000][0.0000 179.2000 0.0000]

Table 38 Data for eighth stiffener in Table 5 (units in mm)

$h_s = 180$ $h_f = 29.52$ $h_w = 150.48$ $t_w = 10$ $t_{bf} = 25$ $r = 7$ $r_1 = (1/10)t_w$=10/10=1 $\alpha = \pi / 6$	[0.0000 0.0000 0.0000][10.0000 0.0000 0.0000][10.0000 150.4833 0.0000][10.9378 153.9833 0.0000][13.5000 156.5455 0.0000][31.5000 166.9378 0.0000][35.0000 173.0000 0.0000][28.0000 180.0000 0.0000][1.0000 180.0000 0.0000][0.2929 179.7071 0.0000][0.0000 179.0000 0.0000]

Table 39 Data for angle stiffener in Figure 9 (units in mm)

$h_s = 120$ $h_{wa} = 107.53$ $t_w = 6$ $t_{bf} = 17$ $t_f = 12.47$	[0 0 0][6 0 0][6 107.5259068 0][23 107.5259068 0][23 120 0][0 120 0]

3. DATA FOR THE STIFFENED PLATE MODELS

Table 40 Data for stiffened plate models 1-3 with no flange (units in inches)

See Table 7 for parameters.	[0.0000 0.0000 3.3233][72.0000 0.0000 3.3233][0.0000 0.0000 0.0000][72.0000 0.0000 0.0000][0.0000 -20.0000 0.0000][72.0000 -20.0000 0.0000][0.0000 20.0000 0.0000][72.0000 20.0000 0.0000]

Table 41 Data for stiffened plate models 4-6 with no flange (units in inches)

See Table 10 for parameters.	[0.0000 0.0000 3.9138][72.0000 0.0000 3.9138][0.0000 0.0000 0.0000][72.0000 0.0000 0.0000][0.0000 -20.0000 0.0000][72.0000 -20.0000 0.0000][0.0000 20.0000 0.0000][72.0000 20.0000 0.0000]

Use the following tables to build the stiffened plate models. In MSC Patran, create the geometry from the points in each table by entering the points and then create the curves and surfaces as appropriate. Create a mesh (with mesh size 1) for the plate and web surfaces. Create a mesh for the curve at the top of the web with topology BAR2. The curve will serve as the flange once the appropriate beam section is created. Using the properties menu, create and name a 1D beam property set. Use the general section (CBEAM) option. Use the input properties button and then the create sections beam library to create and emplace the appropriate flange onto the web. For the bulb-flat flange, use the beam library to create and name a bulb-flat flange by selecting the arbitrary shape button and the boundary loops method button. For the input option, set the select surface option. In the select surface menu, set the maximum allowable curvature error to 0.005. Select the surface and press OK. In the general beam (CBEAM) input properties subordinate menu, enter the appropriate material name,

section name (just created in the create sections beam library), and bar orientation (start by using the vector $\langle 0,1,0 \rangle$ and adjust with $\langle 1,0,0 \rangle$ or $\langle 0,0,1 \rangle$ as needed).

Table 42 Data for bulb-flat stiffened plate model 1b (units in inches)

See Table 7 model 1b for parameters.	[0.0000 -0.1181 3.3233][0.0000 0.1181 3.3233][0.0000 0.1445 3.4217][0.0000 0.2165 3.4938][0.0000 0.6890 3.7665][0.0000 0.7874 3.9370][0.0000 0.5906 4.1339][0.0000 -0.0945 4.1339][0.0000 -0.1112 4.1269][0.0000 -0.1181 4.1102][0.0000 0.0000 3.3233][72.0000 0.0000 3.3233][0.0000 0.0000 0.0000][72.0000 0.0000 0.0000][0.0000 -20.0000 0.0000][72.0000 -20.0000 0.0000][0.0000 20.0000 0.0000][72.0000 20.0000 0.0000]

Table 43 Data for bulb-flat stiffened plate model 2b (units in inches)

See Table 8 model 2b for parameters.	[0.0000 -0.1181 3.3233][0.0000 0.1181 3.3233][0.0000 0.1445 3.4217][0.0000 0.2165 3.4938][0.0000 0.8071 3.8347][0.0000 0.9055 4.0052][0.0000 0.7087 4.2020][0.0000 -0.0945 4.2020][0.0000 -0.1112 4.1951][0.0000 -0.1181 4.1784][0.0000 0.0000 3.3233][72.0000 0.0000 3.3233][0.0000 0.0000 0.0000][72.0000 0.0000 0.0000][0.0000 -20.0000 0.0000][72.0000 -20.0000 0.0000][0.0000 20.0000 0.0000][72.0000 20.0000 0.0000]

Table 44 Data for bulb-flat stiffened plate model 3b (units in inches)

See Table 9 model 3b for parameters.	[0.0000 -0.1181 3.3233][0.0000 0.1181 3.3233][0.0000 0.1445 3.4217][0.0000 0.2165 3.4938][0.0000 1.0039 3.9484][0.0000 1.1024 4.1189][0.0000 0.9055 4.3157][0.0000 -0.0945 4.3157][0.0000 -0.1112 4.3088][0.0000 -0.1181 4.2921][0.0000 0.0000 3.3233][72.0000 0.0000 3.3233][0.0000 0.0000 0.0000][72.0000 0.0000 0.0000][0.0000 -20.0000 0.0000][72.0000 -20.0000 0.0000][0.0000 20.0000 0.0000][72.0000 20.0000 0.0000]

Table 45 Data for bulb-flat stiffened plate model 4b (units in inches)

See Table 10 model 4b for parameters.	[0.0000 -0.1181 3.9138][0.0000 0.1181 3.9138][0.0000 0.1445 4.0123][0.0000 0.2165 4.0843][0.0000 0.6890 4.3571][0.0000 0.7874 4.5276][0.0000 0.5906 4.7244][0.0000 -0.0945 4.7244][0.0000 -0.1112 4.7175][0.0000 -0.1181 4.7008][0.0000 0.0000 3.9138][72.0000 0.0000 3.9138][0.0000 0.0000 0.0000][72.0000 0.0000 0.0000][0.0000 -20.0000 0.0000][72.0000 -20.0000 0.0000][0.0000 20.0000 0.0000][72.0000 20.0000 0.0000]

Table 46 Data for bulb-flat stiffened plate model 5b (units in inches)

See Table 11 model 5b for parameters.	[0.0000 -0.1181 3.9138][0.0000 0.1181 3.9138][0.0000 0.1445 4.0123][0.0000 0.2165 4.0843][0.0000 0.8071 4.4253][0.0000 0.9055 4.5958][0.0000 0.7087 4.7926][0.0000 -0.0945 4.7926][0.0000 -0.1112 4.7857][0.0000 -0.1181 4.7690][0.0000 0.0000 3.9138][72.0000 0.0000 3.9138][0.0000 0.0000 0.0000][72.0000 0.0000 0.0000][0.0000 -20.0000 0.0000][72.0000 -20.0000 0.0000][0.0000 20.0000 0.0000][72.0000 20.0000 0.0000]

Table 47 Data for bulb-flat stiffened plate model 6b (units in inches)

See Table 12 model 6b for parameters.	[0.0000 -0.1181 3.9138][0.0000 0.1181 3.9138][0.0000 0.1445 4.0123][0.0000 0.2165 4.0843][0.0000 1.0039 4.5389][0.0000 1.1024 4.7094][0.0000 0.9055 4.9063][0.0000 -0.0945 4.9063][0.0000 -0.1112 4.8993][0.0000 -0.1181 4.8826][0.0000 0.0000 3.9138][72.0000 0.0000 3.9138][0.0000 0.0000 0.0000][72.0000 0.0000 0.0000][0.0000 -20.0000 0.0000][72.0000 -20.0000 0.0000][0.0000 20.0000 0.0000][72.0000 20.0000 0.0000]

To build the circular flange stiffened plates, ensure a mesh is created for the curve at the top of the web with topology BAR2. The curve will serve as the flange once the appropriate beam section is created. Using the properties menu, create and name a 1D beam property set. Use the general section (CBEAM) option. Use the input properties button and then the create sections beam library button to create and emplace the appropriate flange onto the web. Use the beam library to create and name a flange by selecting the standard shape cross-section using the solid circular shape button with the appropriate radius dimension. In the general beam (CBEAM) input properties subordinate menu, enter the appropriate material name, section name (just created in the create sections beam library), and bar orientation.

Table 48 Data for circular flange stiffened plate model 1c (units in inches)

See Table 7 model 1c for parameters.	[0.0000 0.0000 3.730197][72.0000 0.0000 3.730197][0.0000 0.0000 0.0000][72.0000 0.0000 0.0000][0.0000 -20.0000 0.0000][72.0000 -20.0000 0.0000][0.0000 20.0000 0.0000][72.0000 20.0000 0.0000]

Table 49 Data for circular flange stiffened plate model 2c (units in inches)

See Table 8 model 2c for parameters.	[0.0000 0.0000 3.768468][72.0000 0.0000 3.768468][0.0000 0.0000 0.0000][72.0000 0.0000 0.0000][0.0000 -20.0000 0.0000][72.0000 -20.0000 0.0000][0.0000 20.0000 0.0000][72.0000 20.0000 0.0000]

Table 50 Data for circular flange stiffened plate model 3c (units in inches)

See Table 9 model 3c for parameters.	[0.0000 0.0000 3.831455][72.0000 0.0000 3.831455][0.0000 0.0000 0.0000][72.0000 0.0000 0.0000][0.0000 -20.0000 0.0000][72.0000 -20.0000 0.0000][0.0000 20.0000 0.0000][72.0000 20.0000 0.0000]

Table 51 Data for circular flange stiffened plate model 4c (units in inches)

See Table 10 model 4c for parameters.	[0.0000 0.0000 4.320748][72.0000 0.0000 4.320748][0.0000 0.0000 0.0000][72.0000 0.0000 0.0000][0.0000 -20.0000 0.0000][72.0000 -20.0000 0.0000][0.0000 20.0000 0.0000][72.0000 20.0000 0.0000]

Table 52 Data for circular flange stiffened plate model 5c (units in inches)

See Table 11 model 5c for parameters.	[0.0000 0.0000 4.359019][72.0000 0.0000 4.359019][0.0000 0.0000 0.0000][72.0000 0.0000 0.0000][0.0000 -20.0000 0.0000][72.0000 -20.0000 0.0000][0.0000 20.0000 0.0000][72.0000 20.0000 0.0000]

Table 53 Data for circular flange stiffened plate model 6c (units in inches)

See Table 12 model 6c for parameters.	[0.0000 0.0000 4.422005][72.0000 0.0000 4.422005][0.0000 0.0000 0.0000][72.0000 0.0000 0.0000][0.0000 -20.0000 0.0000][72.0000 -20.0000 0.0000][0.0000 20.0000 0.0000][72.0000 20.0000 0.0000]

To build the T-flange stiffened plate models, the same data in Table 54 is used to build T-flange stiffened plate models 1t, 2t, and 3t. The same data in Table 55 is used to build T-flange stiffened plate models 4t, 5t, and 6t. Ensure a mesh is created for the curve at the top of the web with topology BAR2. The curve will serve as the flange once the appropriate beam section is created. Using the properties menu, create and name a 1D beam property set. Use the general section (CBEAM) option. Use the input properties button and then the create sections beam library button to create and emplace

the appropriate flange onto the web. In the beam library, create and name a standard shape cross-section using the solid rectangular shape button with the appropriate dimensions. In the general beam (CBEAM) input properties subordinate menu, enter the appropriate material name, section name (just created in the create sections beam library), and bar orientation (start by using the vector $\langle 0,1,0 \rangle$ and adjust with $\langle 1,0,0 \rangle$ or $\langle 0,0,1 \rangle$ as needed).

Table 54 Data for T-flange stiffened plate models 1t, 2t, and 3t (units in inches)

See Table 7 model 1t, Table 8 model 2t, or Table 9 model 3t as appropriate for parameters.	[0.0000 0.0000 3.4414][72.0000 0.0000 3.4414][0.0000 0.0000 0.0000][72.0000 0.0000 0.0000][0.0000 -20.0000 0.0000][72.0000 -20.0000 0.0000][0.0000 20.0000 0.0000][72.0000 20.0000 0.0000]

Table 55 Data for T-flange stiffened plate model 4t, 5t, and 6t (units in inches)

See Table 10 model 4t, Table 11 model 5t, or Table 12 model 6t as appropriate for parameters.	[0.0000 0.0000 4.031951][72.0000 0.0000 4.031951][0.0000 0.0000 0.0000][72.0000 0.0000 0.0000][0.0000 -20.0000 0.0000][72.0000 -20.0000 0.0000][0.0000 20.0000 0.0000][72.0000 20.0000 0.0000]

THIS PAGE INTENTIONALLY LEFT BLANK

LIST OF REFERENCES

1. Bleich, F., *Buckling Strength of Metal Structures*, McGraw-Hill Book Co., 1952.
2. Chajes, Alexander, *Principles of Structural Stability Theory*, Prentice-Hall, Inc., 1974.
3. Chou, S. K. G., *Design of Longitudinally Stiffened Plating in Compression with Particular Reference to Torsional Buckling*, Ph.D. Thesis, Civil Engineering Dept., Imperial College, London, August 1997.
4. Corus Group, "Bulb flats", [http://www.corus-specialprofiles.com/pdf/Bulbflat.pdf]. September 2002.
5. Danielson, D. A., "Theory of Shell Stability", *Thin-Shell Structures*, pp. 45-58, 1974.
6. Danielson, D. A., Kihl, D.P., and Hodges, D.H., "Tripping of Thin-Walled Plating Stiffeners in Axial Compression", *Thin-Walled Structures*, Vol. 10, pp. 121-142, 1990.
7. Danielson, D. A., Cricelli, A.S., Frenzen, C.L., and Vasudevan, N., "Buckling of Stiffened Plates Under Axial Compression and Lateral Pressure", *Int. J. Solids Structures*, Vol. 30, No. 4, pp 545-551, 1993.
8. Danielson, D. A., Steele, C. R., Fakhroo, F. and Cricelli, A. S., *Stresses in Ship Plating*, Naval Postgraduate School Technical Report NPS-94-008, 1994.
9. Danielson, D.A., Analytical Tripping Loads for Stiffened Plates, *Int. J. Solids Structures*, Vol. 32, No. 8/9, pp. 1319-1328, 1995.
10. Donaldson, B. K., *Analysis of Aircraft Structures: An Introduction*, McGraw-Hill, Inc., 1993.
11. Henrici, P., *Applied and Computational Complex Analysis, Volume 1, Power Series-Integration-Conformal Mapping-Location of Zeros*, John Wiley & Sons, 1974.
12. Jaeger, L. G., *Elementary Theory of Elastic Plates*, Pergamon Press, 1964.
13. Langhaar, H. L., *Energy Methods in Applied Mechanics*, John Wiley and Sons, Inc., 1962.
14. Naval Postgraduate School Technical Report NPS-MA-96-002, *Buckling of Ship Grillages,* by D. Danielson and D.P. Kihl, September 1996.

15. Naval Postgraduate School Technical Report NPS-MA-97-005, *Buckling of Ship Grillages - Part II,* by D. Danielson and D.P. Kihl, September 1997.
16. Oden, J. T., *Mechanics of Elastic Structures*, McGraw-Hill Book Co., 1967.
17. Paik, J. K. and Kim, B. J., "Ultimate Strength Formulations for Stiffened Plates Under Combined Axial Load, In-Plane Bending and Lateral Pressure: A Benchmark Study", *Thin-Walled Structures*, Vol. 40, pp.45-83, 2002.
18. Pilkey, W. D. and Chang, P.Y., *Modern Formulas for Static and Dynamics: A Stress-and-Strain Approach*, McGraw-Hill Book Co. 1978.
19. Sokolnikoff, I. S., *Mathematical Theory of Elasticity*, 2nd ed., McGraw-Hill Book Co., Inc., 1956.
20. Stakgold, I., *Green's Functions and Boundary Value Problems*, 2nd ed., John Wiley & Sons, Inc., 1998.
21. Timoshenko, S. P. and Gere, J. M., *Theory of Elastic Stability*, 2nd ed., McGraw-Hill Book Co., 1961.
22. Timoshenko, S. P. and Goodier, J. N., *Theory of Elasticity*, 3rd ed., McGraw-Hill Book Co., 1970.
23. Ugural, A. C., *Stresses in Plates and Shells*, McGraw-Hill, Inc., 1981.
24. Washizu, K., *Variational Methods in Elasticity and Plasticity*, 3rd ed., Pergamon Press, 1982.

INITIAL DISTRIBUTION LIST

1. Defense Technical Information Center
   Ft. Belvoir, Virginia

2. Dudley Knox Library
   Naval Postgraduate School
   Monterey, California

3. Dr. Don Danielson
   Naval Postgraduate School
   Monterey, California

4. Dr. Young Kwon
   Naval Postgraduate School
   Monterey, California

5. Dr. David Canright
   Naval Postgraduate School
   Monterey, California

6. Dr. Fariba Fahroo
   Naval Postgraduate School
   Monterey, California

7. Dr. Wei Kang
   Naval Postgraduate School
   Monterey, California

8. Dr. David Kihl
   Naval Surface Warfare Center
   West Bethesda, Maryland

9. Geoff Lofthouse
   Corus Group
   Skinningrove, United Kingdom